

Trust-informed Decision-Making Through An Uncertainty-Aware Stacked Neural Networks Framework Case Study in COVID-19 Classification

Hassan Gharoun¹, Mohammad Sadegh Khorshidi¹, Fang Chen¹, and Amir H. Gandomi^{1,2,3}

Abstract—This study presents an uncertainty-aware stacked neural networks model for the reliable classification of COVID-19 from radiological images. The model addresses the critical gap in uncertainty-aware modeling by focusing on accurately identifying confidently correct predictions while alerting users to confidently incorrect and uncertain predictions, which can promote trust in automated systems. The architecture integrates uncertainty quantification methods, including Monte Carlo dropout and ensemble techniques, to enhance predictive reliability by assessing the certainty of diagnostic predictions. Within a two-tier model framework, the tier one model generates initial predictions and associated uncertainties, which the second tier model uses to produce a trust indicator alongside the diagnostic outcome. This dual-output model not only predicts COVID-19 cases but also provides a trust flag, indicating the reliability of each diagnosis and aiming to minimize the need for retesting and expert verification. The effectiveness of this approach is demonstrated through extensive experiments on the COVIDx CXR-4 dataset, showing a novel approach in identifying and handling confidently incorrect cases and uncertain cases, thus enhancing the trustworthiness of automated diagnostics in clinical settings.

Index Terms—Uncertainty-aware, Trust-informed, Uncertainty quantification, Monte-Carlo dropout, Ensemble, COVID-19, Artificial neural networks.

I. INTRODUCTION

THE COVID-19 pandemic affected numerous countries, leading to millions of cases and fatalities worldwide. Detecting and diagnosing COVID-19 at an early stage proved to be crucial in controlling its spread [1]. Rapid diagnosis facilitated timely medical intervention and recovery. Alongside polymerase chain reaction (PCR) tests, chest radiography (X-rays) and computed tomography (CT) scans were employed as key diagnostic tools. Due to the limited availability of PCR tests in many regions, medical imaging emerged as a primary method for diagnosing COVID-19 [1]. As a standard procedure, these images required manual analysis by clinical experts. However, the ongoing shortage of healthcare professionals, especially in developing nations and smaller hospitals, made quick diagnosis challenging and exacerbated the workload on existing experts. At this moment, the advantages of AI became more obvious in healthcare.

However, it appears that no AI-based healthcare tools have been officially incorporated into clinical guidelines as

a standard part of medical practice [2]. A critical factor that hinders AI acceptance and adoption among both healthcare professionals and patients is the lack of *trust* in the decisions made by AI systems [3].

Numerous studies have investigated the underlying factors contributing to the persistent challenge of establishing trust in AI within the healthcare domain, and several key factors have been identified [3]. One major factor contributing to the lack of trust in AI systems is their inconsistent performance across different clinical settings [4]. This inconsistent performance can be interpreted as uncertainty in machine learning (ML) and AI predictions.

Uncertainty mainly originates from two sources [5]: (I) data uncertainty, which is due to elements such as noise, complexity, and limited knowledge about environmental conditions (aleatoric uncertainty), and (II) parametric uncertainty, which occurs when the model is inadequate because of imprecise understanding of its components (epistemic uncertainty). The presence of various sources of uncertainty requires a model to explicitly assert the certainty of its outputs to establish its reliability and trustworthiness. For this purpose, uncertainty quantification techniques have been developed to assess and communicate the confidence levels associated with the model's predictions. The quantified uncertainty serves as a metric, where values above a specific threshold are flagged as uncertain, while those below the threshold are deemed certain. Ideally, in an optimally calibrated machine learning model, the quantified uncertainty for all correct predictions would fall below this threshold (indicating certainty or confidence), and for all incorrect predictions, it would exceed the threshold (indicating uncertainty). However, incorrect predictions could also fall below this threshold, leading to confidently incorrect predictions. This conventional approach, where confidently incorrect predictions are not adequately addressed, exacerbates the erosion of trust in ML and AI, particularly in high-stakes fields such as medical diagnosis.

Therefore, this study proposes an expressive uncertainty-aware model with a dual output: (1) the predicted outcome and (2) a binary flag indicating whether the outcome should be trusted. This second flag is specifically designed to mark only confidently correct predictions as trustworthy, thereby helping to avoid confidently incorrect predictions. This second output enables the model to flag predictions (especially in medical diagnosis within healthcare) with a "do not trust me" alert, prompting human experts (such as physicians) to re-evaluate them. Thus, the model not only enhances user experience but also fosters greater adoption by encouraging cautious and

¹Faculty of Engineering & IT, University of Technology Sydney, e-mails: Hassan.Gharoun@student.uts.edu.au, MS.khorshidialikordi@student.uts.edu.au, Fang.Chen@uts.edu.au, Gandomi@uts.edu.au.

²University Research and Innovation Center (EKIK), Óbuda University.

³Corresponding author

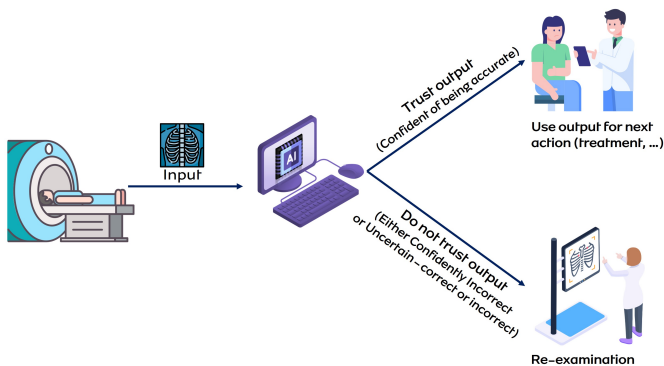


Fig. 1: Uncertainty-informed diagnosis Schema.

trust-informed decision-making. The process of trust-informed medical diagnosis is illustrated in Figure 1.

The rest of the paper is organized as follows: Section II reviews relevant previous research and outlines the contributions of this study. Section III provides a detailed exploration of the proposed algorithm. Sections IV and V explain the dataset used and describe the experimental framework respectively. Insights and analysis from the experiments are presented in Section VI. Finally, Section VII offers concluding remarks and suggests directions for future research.

II. BACKGROUND

ML including neural networks (NNs) have reached a peak in accuracy. Individuals may misinterpret high accuracy as indicating high confidence, based on their intuitive understanding of probabilities. In classification problems, a frequent misunderstanding of ‘confidence’ arises when the probability assigned to a predicted class is mistaken as a true measure of the model’s certainty. This is misleading because these probability scores, especially in NNs, are typically calculated using the Softmax function, which normalizes outputs to represent class probabilities rather than confidence levels [6].

To evaluate confidence or its inverse, uncertainty, it is crucial to recognize that most conventional ML models, including NNs, typically generate deterministic predictions by producing a single output, or point estimate, for a given input [7]. This approach is not able to capture the variability (or in other words uncertainty) in the model’s predictions.

To illustrate this, consider a neural network f parameterized by \mathbf{w} , which maps an input $\mathbf{x} \in \mathcal{X}$ to an output $y \in \mathcal{Y}$. The target output is obtained by optimizing the parameters of the network, such that $y = f_{\mathbf{w}}(\mathbf{x})$. Rather than relying on point estimation for \mathbf{w} , assigning a probability distribution over the model parameters enables the derivation of a probability distribution for predictions, allowing for the quantifying uncertainty regarding the model’s knowledge (referred to as epistemic uncertainty). Bayesian inference methods - including Markov chain Monte Carlo (MCMC) [8], Variational inference (VI) [9], Monte Carlo dropout (MCD) [6], Variational Autoencoders (VAE) [10], Bayes By Backprop (BBB) [11] - are commonly employed to estimate the posterior distribution of the model parameters to achieve this. In addition to Bayesian

techniques, ensemble learning is another method frequently used to quantify uncertainty. In a typical ensemble, each model independently predicts the output for a given input. When these models are diverse—built with different architectures, parameters, or trained on various data subsets—they produce probabilistic predictions instead of single-point estimates. For further details on uncertainty quantification techniques, interested readers can refer to [5].

By leveraging the aforementioned uncertainty quantification (UQ) methods, there has been a growing interest in the development of uncertainty-aware ML models, particularly NNs. These research efforts can be categorized into two main categories:

The first category of studies emphasizes quantifying uncertainty to enhance decision-making by communicating prediction uncertainties. Typically, these studies generate predictions accompanied by uncertainty estimates using one of the aforementioned UQ methods. Predictions with the highest uncertainty are flagged as potentially inaccurate, enabling more informed and cautious decision-making. Among these studies, MCD is widely employed in healthcare to quantify uncertainty and improve decision-making. For instance, in cardiac arrhythmia detection, gated recurrent neural networks (GRUs) with MCD provide well-calibrated uncertainty estimates, crucial for clinical confidence [7]. Similarly, deep learning models with MCD are utilized for stroke outcome prediction, helping to identify high-risk predictions that necessitate further human evaluation [12]. Another application involves the multi-level context and uncertainty aware (MCUa) model for breast histology. The model uses context-aware networks to learn spatial dependencies among image patches and applies MCD to measure confidence levels based on the standard deviation of multiple predictions. Lower standard deviations are interpreted as higher confidence, and predictions with low uncertainty are selected as confident. [13]. Furthermore, MCD enhances colorectal polyp classification by utilizing predictive variance and entropy for uncertainty measurement, along with temperature scaling for confidence calibration [14]. Application of MCD is not limited to health care and in the domain of credit card fraud detection, MCD combined with ensemble methods quantifies prediction uncertainty, thereby enhancing the clarity of the system’s reliability in the detection process [15].

While MCD is a popular choice in healthcare, Bayesian deep learning techniques have found application across a wider range of domains, providing robust uncertainty quantification. In engineering applications, Bayesian neural networks (BNNs) and stochastic variational Gaussian processes (SVGPs) are used for building energy modeling, providing predictions with confidence intervals that optimize resource allocation and enhance model robustness [16]. In nuclear power plants, Bayesian models estimate predictive uncertainty to enhance decision-making and risk management in health monitoring systems [17]. Another study leverages Bayesian networks in agribusiness risk assessment to quantify uncertainty and improve out-of-domain calibration, aiding financial decision-making [18]. Furthermore, in transformer diagnostics, Gaussian Bayesian networks (GBNs) are combined with black-

box classifiers to quantify uncertainty, leveraging the strengths of different models to improve diagnostic accuracy through probabilistic predictions [19].

In addition to MCD and Bayesian approaches, ensemble learning methods are prominently used for uncertainty quantification, particularly in high-stakes environments where reliability is paramount. A framework for COVID-19 diagnosis employs pre-trained convolutional neural networks (CNNs) like VGG16 and ResNet50, extracting features from chest X-rays and CT images while estimating epistemic uncertainty through model ensembles to ensure higher accuracy and reliability [20]. In defect detection for casting products, transfer learning with CNNs and deep learning ensembles is used to estimate epistemic uncertainty, improving model trustworthiness by identifying poorly trained input regions [21]. In food recognition tasks, epistemic uncertainty guides the selection of ensemble models, enhancing accuracy and robustness by choosing diverse models with low mean uncertainty [22].

The second category of studies goes beyond merely quantifying uncertainty, incorporating it directly into the training process to enhance the model's confidence. Typically, these approaches introduce new loss functions that are designed around uncertainty estimations, allowing the model to better account for uncertainty during learning.

A notable approach by [23] introduced a multi-objective loss function that simultaneously optimizes prediction accuracy and uncertainty estimates. This loss function combines cross-entropy with Kullback-Leibler (KL) divergence to measure the separation between uncertainty densities for correct and incorrect predictions. Applied to datasets like COVID-19 and breast cancer, this approach enhances reliability by improving accuracy and calibrating uncertainty estimates.

Similarly, [24] developed a framework for breast cancer assessments that addresses labeling ambiguity by converting deterministic tumor cellularity labels into probabilistic distributions. The learning process is guided by minimizing the Kullback-Leibler divergence between predicted and true label distributions, thus integrating uncertainty directly into the model's training. In a related effort, [25] designed a novel loss function for skin cancer diagnosis that penalizes overconfident mistakes. By leveraging MCD for UQ, the loss function combines traditional binary cross-entropy with predictive entropy to enhance calibration and uncertainty awareness, ensuring that overconfident predictions do not compromise clinical decision-making.

Further advancements include introducing two new loss functions, predictive entropy (PE) and expected calibration error (ECE)-based Loss functions by using MCD. The PE-based loss function minimizes uncertainty for correct predictions and increases it for incorrect ones, while the ECE-based loss function improves calibration by aligning model confidence with accuracy [26]. [27] explored the use of deterministic uncertainty models in cardiac imaging, proposing two new loss functions—accuracy versus uncertainty (AvUC) loss and maximum mean calibration error (MMCE) loss. These functions, which are embedded within evidential neural networks (ENNs) and deep deterministic uncertainty (DDU) networks, balance model confidence with accuracy, ensuring that the

model's predicted confidence aligns closely with its actual performance. In another study, [28] further integrated both aleatoric and epistemic uncertainties into the training process. Aleatoric uncertainty is estimated through data augmentation and inference-time dropout, while epistemic uncertainty is quantified by sampling latent representations from the VAE. Both uncertainties guide training via (a) paired confidence loss, which adjusts the model to boost confidence in correct predictions and reduce confidence in incorrect ones, and (b) the confidence weighting function, which penalizes overconfident incorrect predictions, improving calibration by aligning prediction confidence with actual accuracy.

The refinement of UQ has also been approached through the introduction of uncertainty-weighted metrics. [29] applied a quadratic weighted Cohen's kappa (QWK)-based uncertainty measure in the context of diabetic retinopathy classification. This metric aligns uncertainty with clinical performance, prioritizing the reduction of significant misclassifications by penalizing larger errors more heavily. Lastly, [30] proposed a method combining similarity and sensitivity analysis to refine uncertainty quantification. This approach begins with a shallow neural network to capture initial predictions and estimate uncertainties, followed by a sensitivity analysis to identify inputs contributing to uncertainty. The method culminates in refining prediction intervals through a bound correction network, thereby enhancing model robustness.

The review of research within the first category demonstrates that uncertain predictions can be effectively identified. Insights from the second category highlight that quantified uncertainty can be leveraged as an uncertainty-based loss function, which, when integrated with traditional error-based loss functions, enhances model performance in terms of both accuracy and uncertainty estimation. However, both categories of research primarily adhere to the conventional practice of applying an uncertainty threshold, wherein predictions with quantified uncertainty exceeding the threshold are flagged for further review, while those below it are accepted. To the best of the authors' knowledge, none of these studies—despite introducing novel uncertainty-based loss functions for calibration—ensures the complete elimination of confidently incorrect predictions. Furthermore, the prevailing method of merely comparing quantified uncertainty against a set threshold is inherently insufficient for reliably detecting such confidently incorrect predictions. In the high-stakes field of healthcare, if physicians and patients encounter confidently incorrect outcomes, especially in medical diagnosis applications, trust in AI and ML systems can be severely undermined. Furthermore, misclassifying a disease as a healthy condition may result in missing the optimal treatment window, leading to serious consequences [31]. Accordingly, this study aims to address this challenge by proposing a stacked neural networks architecture designed to identify predictions that the model is highly confident in being correct. The model provides two outputs: the predicted label and a trust indicator for that prediction. The proposed architecture enables the model to learn to identify both confidently incorrect and uncertain predictions, ensuring that only confidently correct predictions are trusted.

III. METHODOLOGY

Stacked generalization, commonly known as stacking, is a robust ML technique that involves two distinct levels of models: the base models (level-0) and the meta-model (level-1). In the first level, various algorithms, which can be either heterogeneous (different types of models) or homogeneous (same type of models) [32], are trained on the original training dataset. These base models generate predictions which are then used as input features for the meta-model. The meta-model’s purpose is to learn the optimal way to combine these base models’ predictions to achieve the best possible performance [33]. Additionally, the meta-model can also incorporate the original input features from the training data alongside the base model outputs to enhance its learning process.

This study draws upon the concept of traditional stacking models to propose a new architecture that, while resembling stacking, serves a different purpose: trust-informed prediction.

In the proposed method, while maintaining a similar two-level architecture (level-0 for the base model and level-1 for the meta-model), the meta-model’s objective is different. Here, the meta-model aims to learn the relationship between the base-model predictions and their associated uncertainties. Consequently, the output of the meta-model is a flag that indicates whether the model’s prediction is trustworthy or not. To align with this new objective, the architecture of the proposed method is described in detail in the following sections.

A. Uncertainty-Aware Stacked Neural Networks

Figure 2 illustrates the overall flow of the uncertainty-aware stacked neural networks (U-SNN) framework, which is architected with two integrated layers: the Level 0 base model as the initial predictor and the Level 1 meta-model as the trust evaluator. This study applies the U-SNN framework to the classification task, beginning with a dataset $D = \{(x_1, y_1), (x_2, y_2), \dots, (x_N, y_N)\}$, where x_i and y_i represent the i^{th} observation vector and its corresponding label in a d -dimensional feature space. The initial step involves splitting the dataset into training and testing subsets, denoted as D_{train} and D_{test} , respectively. In this study, D_{train} is exclusively used for training both the base model and the meta-model, while D_{test} is reserved solely for evaluating the performance of the proposed method. This approach ensures that the base and meta-models do not have access to or influence from the test dataset, thereby providing an unbiased assessment of the proposed method.

The base model classifier generates class predictions, with the associated uncertainty estimations used to construct a new training set for the meta-model. For clarity, this second training set is referred to as the meta-train set. The uncertainty estimations of the base model in this study are calculated using three distinct UQ techniques: (1) MCD, (2) Ensemble, and (3) Ensemble Monte Carlo dropout (EMCD). Detailed descriptions of each technique are provided in the subsequent section III-B.

Following the training of the base model, the meta-train set is constructed by combining the original input features X_i

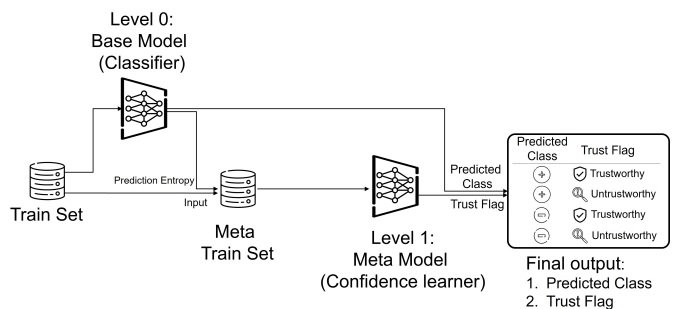


Fig. 2: Uncertainty-aware Stacked Neural Networks (U-SNN) Schema.

with the estimated uncertainty e_i as an additional independent variable.

The target variable of the meta-train set is a binary label z_i derived as follows:

$$z_i = \begin{cases} 1 & \text{if } \hat{y}_i = y_i \text{ and } e_i \leq \tau \\ 0 & \text{otherwise} \end{cases} \quad (1)$$

Where:

- \hat{y}_i : Predicted label for the i^{th} instance
- y_i : Ground truth for the i^{th} instance
- e_i : estimated prediction’s uncertainty for the i^{th} instance
- τ : Confidence threshold.
- z_i : Binary label for the i^{th} instance, with 1 indicating ”Trustworthy” and 0 indicating ”Untrustworthy”.

Eq. 1 reflects the primary objective of the meta-model, which is to identify instances where the model’s predictions are both correct and confident ($z_i = 1$). This conservative approach ensures that only predictions with high confidence and accuracy are trusted, while confidently incorrect predictions and uncertain predictions—whether correct or incorrect—are flagged as untrustworthy ($z_i = 0$) and marked for further investigation.

In this study, prediction entropy (PE) is chosen as the sole metric indicator of prediction uncertainty. Therefore, in the Eq. 1, the estimated uncertainty e_i denotes the PE. PE ranges between 0 and 1, with values closer to zero indicating lower entropy, and thus lower uncertainty and higher confidence, while values closer to 1 indicate higher entropy, greater uncertainty, and lower confidence. Consequently, a lower confidence threshold is more strict, as it allows only correct predictions with a PE lower than the τ to be flagged as trustworthy.

The following outlines the calculation of PE using the three different UQ methods employed in this study.

B. Uncertainty Quantification Methods

1) *Monte-Carlo Dropout (MCD)*: Building on the concepts of UQ outlined in the section II, MCD is implemented to approximate Bayesian inference in deep neural networks. Dropout originally designed as a regularization technique to prevent overfitting by randomly deactivating a subset of neurons during training.

This process can be adapted for uncertainty estimation by applying dropout during the inference stage. By performing multiple forward passes through the network with dropout enabled during inference, each pass results in slightly different predictions due to the random dropout of neurons, thereby producing a distribution of outputs for a given input. Each neuron in the network effectively samples from a Bernoulli distribution, and the collection of predictions across multiple stochastic forward passes serves as a Monte Carlo approximation of the posterior distribution.

Here, PE as an uncertainty evaluation metric is calculated as follows 2:

$$PE(\mathbf{x}) = - \sum_{c=1}^C \mu_{\text{pred}}(\mathbf{x}, c) \log[\mu_{\text{pred}}(\mathbf{x}, c)] \quad (2)$$

Eq. 2 represents the prediction entropy $PE(\mathbf{x})$, calculated over C classes, where $\mu_{\text{pred}}(\mathbf{x}, c)$ denotes the mean predicted probability of class c for the input \mathbf{x} calculated as Eq. 3:

$$\mu_{\text{pred}}(x, c) = \frac{1}{M} \sum_{m=1}^M p(y = c | x, \omega_m) \quad (3)$$

where $p(y = c | x, \omega_m)$ denotes the probability that the input x is assigned to class c , as determined by the softmax function, using the set of parameters ω_m from the m^{th} iteration of the model, and M signifies the count of such iterations.

2) *Ensemble*: In an ensemble of neural networks, each model independently computes a prediction for the same input. The diversity among these models, which can arise from differences in architecture and parameters leads to a range of predictions. The variation of these predictions highlights epistemic uncertainty, representing the model's uncertainty due to incomplete knowledge. A greater variation in the predictions signals more significant uncertainty, indicating that the models do not agree, while a lesser variation suggests a higher confidence in the predicted outcome. PE in ensemble setting is calculated as 4:

$$PE(\mathbf{x}) = - \sum_{c=1}^C \mu_{\text{pred}}(\mathbf{x}, c) \log[\mu_{\text{pred}}(\mathbf{x}, c)] \quad (4)$$

Eq. 4 describes the prediction entropy $PE(\mathbf{x})$ for ensemble methods, where $\mu_{\text{pred}}(\mathbf{x}, c)$ indicates the mean predicted probability of class c for the input \mathbf{x} , derived as shown in Eq. 5:

$$\mu_{\text{pred}}(\mathbf{x}, c) = \frac{1}{N} \sum_{n=1}^N p(y = c | \mathbf{x}, \theta_n) \quad (5)$$

In Eq. 5, $p(y = c | \mathbf{x}, \theta_n)$ is the probability that the input \mathbf{x} belongs to class c , computed by the softmax function using the parameters θ_n of the n^{th} model in the ensemble, and N is the total number of models in the ensemble.

3) *Ensemble Monte-Carlo Dropout (EMCD)*: The integration of ensemble methods with MCD (EMCD) offers a dual approach to uncertainty quantification. In this setting, each neural network within the ensemble applies dropout during the inference phase, not just during training. This process results in a varied set of predictions for each model, collectively contributing to a broader distribution of predictions. PE for this approach is calculated to measure the dispersion of predictions across the ensemble and across multiple stochastic passes for each model. The formula for PE is given by:

$$PE(\mathbf{x}) = - \sum_{c=1}^C \bar{\mu}_{\text{pred}}(\mathbf{x}, c) \log[\bar{\mu}_{\text{pred}}(\mathbf{x}, c)] \quad (6)$$

Here, $\bar{\mu}_{\text{pred}}(\mathbf{x}, c)$ represents the mean predicted probability of class c for the input \mathbf{x} , computed across all models in the ensemble and all dropout iterations:

$$\bar{\mu}_{\text{pred}}(\mathbf{x}, c) = \frac{1}{NM} \sum_{n=1}^N \sum_{m=1}^M p(y = c | \mathbf{x}, \omega_{nm}) \quad (7)$$

In this expression, $p(y = c | \mathbf{x}, \omega_{nm})$ is the probability that the input \mathbf{x} is classified as class c , using the set of parameters ω_{nm} during the m^{th} Monte Carlo iteration of the n^{th} model in the ensemble. N is the number of models in the ensemble, and M represents the number of Monte Carlo iterations per model.

C. Evaluation Metrics

Considering the proposed two-level architecture, traditional error-based performance metrics (such as the F1 score) for each model individually assess their training effectiveness but fail to provide a comprehensive evaluation of the entire framework's performance. To gain a holistic understanding, it is essential to integrate the outputs of both the base and meta-models.

Thus, new quantitative performance metrics have been proposed to evaluate trust-informed predictions (based on uncertainty estimations) by combining the outputs of both models, in a manner analogous to the traditional confusion matrix. In the context of binary classification, the base model's predictions are compared with the ground truth labels, resulting in four categories: true positive (TP), false positive (FP), true negative (TN), and false negative (FN). Concurrently, the meta-model's predicted confidence labels are compared with the ground truth trustworthy labels, yielding four additional categories: true trustworthy (TT), false trustworthy (FT), true untrustworthy (TU), and false untrustworthy (FU). By integrating these correctness and confidence classifications, 16 distinct outcomes are generated, as illustrated in Table I. For ease of reference, the proposed confusion matrix is called the trust-informed confusion matrix.

TABLE I: Trust-informed Confusion Matrix

		U-SNN Output					
		Positive			Negative		
		Trustworthy	Untrustworthy	Trustworthy	Untrustworthy		
Ground Truth	Positive	Trustworthy	TPTT	TPFU	FNFT	FNFU	
		Untrustworthy	TPFT	TPTU	FNFT	FNFTU	
	Negative	Trustworthy	FPFT	FPFU	TNFT	TNFU	
		Untrustworthy	FPFT	FPTU	TNFT	TNTU	

In the proposed trust-informed confusion matrix, four combinations—FNNT, FPTT, FNFU, and FPFU—never occur. This exclusion is rooted in the definition of the meta-train set target variable as described in Eq. 1. As per this definition, incorrect predictions are never classified as trustworthy; hence, false positives and false negatives cannot be designated as true trustworthy (TT). Furthermore, since incorrect predictions cannot qualify as true trustworthy, they are also precluded from being classified as false untrustworthy (FU).

Considering the proposed confusion matrix, optimal performance is achieved when the model confidently makes correct predictions and is uncertain when an incorrect decision is likely. This means the model should never confidently make an incorrect prediction, and conversely, should never be uncertain when making a correct prediction. The idea is that when the model flags a prediction as uncertain, it should be reviewed by an expert for further examination. For the model to be efficient, only a small percentage of predictions—those where the model is unlikely to be accurate (i.e., where the model recognizes its own incorrectness)—should be flagged for further review. This approach minimizes the workload for expert review while maintaining high reliability.

Building upon the trust-informed confusion matrix, several quantitative criteria have been established as follows. These criteria are designed to evaluate how closely the model adheres to the optimal performance principles described above. These criteria are:

- **Confident Accuracy Rate (CAR):** CAR is a metric that quantifies the proportion of instances where the model is accurate and confident, indicating its trustworthiness. It is defined as Eq. 8. The rationale behind naming this ratio *Confident Accuracy* lies in the definition of the meta-train set target variable as "trustworthy," as described in Eq. 1. In this context, "trustworthy" signifies predictions that are both correct and made with high confidence. Generally, a higher CAR is desirable.

$$CAR = \frac{TPPT + TNTT}{Total\ Outcomes} \quad (8)$$

- **Confident Precision Rate (CPR):** CPR is a metric that measures the proportion of accurate predictions flagged as trustworthy, formulated by Eq. 9. Similarly, the rationale behind naming this ratio *Confident Precision* lies in the fact that this metric captures the percentage of correct predictions made with high confidence (which, according to the Eq. 1, are flagged as trustworthy) among all correct predictions. A CPR close to 1 is desirable, indicating that the model's confident predictions are almost always correct.

$$CPR = \frac{TPPT + TNTT}{TAP} \quad (9)$$

where TAP stands as total accurate predictions defined by Eq. 10:

$$TAP = TPPT + TPFU + TPFT + TPTU + TNTT + TNFU + TNFT + TNTU \quad (10)$$

- **Trust Precision Rate (TPR):** TPR is a metric that measures the proportion of predictions flagged as trustworthy that are actually trustworthy, formulated by Eq. 11. A TPR close to 1 is desirable. Naturally, $1 - TPR$ represents the percentage of records that the model erroneously flags as trustworthy.

$$TPR = \frac{TPPT + TNTT}{TTP} \quad (11)$$

where TTP stands as total trustworthy predictions defined by Eq. 12:

$$TTP = TPPT + FNNT + FPTT + TNTT + TPFT + FNFT + FPFT + TNFT \quad (12)$$

- **False Trust Rate (FTR):** FTR measures the proportion of incorrect predictions that the model has erroneously classified as trustworthy. This measure is crucial in applications where false trust in incorrect predictions could lead to significant consequences. A lower FTR is desirable, as it indicates fewer instances where the model's incorrect predictions are mistakenly trusted. The FTR is defined as Eq. 13:

$$FTR = \frac{FPFT + FNFT}{Total\ Outcomes} \quad (13)$$

- **Review Alert Ratio (RAR):** RAR is a metric that measures the proportion of predictions flagged as untrustworthy, requiring expert review, represented by Eq. 14. This metric encompasses all untrustworthy predictions, irrespective of whether they genuinely necessitate review or are incorrectly flagged as untrustworthy. A high RAR signifies inefficiency, indicating that a larger proportion of instances are being flagged for review, thereby increasing the review burden.

$$RAR = \frac{TUP}{Total\ Outcomes} \quad (14)$$

where TUP is defined as total untrustworthy predictions as Eq. 15:

$$TUP = TPFU + TPTU + FNFU + FNTU + FPFU + FPTU + TNFU + TNTU \quad (15)$$

- **Miscalibration Review Ratio (MRR):** MRR quantifies the proportion of predictions flagged for review due to the base model's miscalibration. Specifically, it measures the rate at which the base model, despite being correct, has low confidence (indicating a miscalibration in the base model's confidence assessment) and thus flags predictions as untrustworthy. A lower MRR indicates better calibration of the base model's confidence with its actual predictive accuracy. The MRR is defined as Eq. 16:

$$MRR = \frac{TPTU + TNTU}{TUP} \quad (16)$$

- **True Review Ratio (TRR):** TRR is a metric that quantifies the proportion of instances where the model correctly identifies its incorrect predictions and flags them as untrustworthy formulated by Eq. 17. This metric indicates

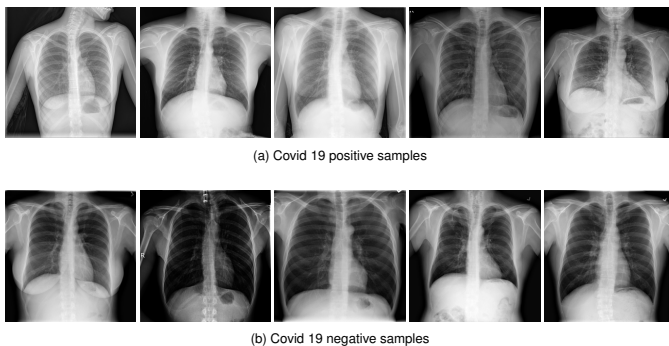


Fig. 3: Examples images from COVIDx CXR-4 dataset.

the model’s ability to recognize and appropriately flag its own errors. A TRR close to 1 is desirable, indicating that the model effectively flags only incorrect instances as untrustworthy.

$$TRR = \frac{FNTU + FPTU}{TUP} \quad (17)$$

- False Review Ratio (FRR): FRR quantifies the proportion of correct predictions that are incorrectly flagged as untrustworthy due to a meta-model error, thereby requiring unnecessary review, as formulated in Eq. 18. An FRR close to 0 is desirable.

$$FRR = \frac{TPFU + TNFU}{TUP} \quad (18)$$

IV. DATA SETS

The dataset utilized in the study is COVIDx CXR-4 [34], an expanded multi-institutional open-source benchmark dataset specifically designed for chest X-ray image-based computer-aided COVID-19 diagnostics. This dataset significantly expands upon its predecessors, the COVIDx CXR datasets, by increasing the total patient cohort size to 84,818 images from 45,342 patients across multiple institutions. The age distribution of the patients ranges widely, though there is a notable bias, with over half of the patients being between 18 and 59 years old. Additionally, the dataset maintains a nearly equal gender distribution and varied imaging views. The COVIDx CXR-4 dataset includes two main classes: positive COVID-19 cases and negative cases. Among the 84,818 images, 65,681 are positive COVID-19 cases, while 19,137 are negative cases, reflecting a significant class imbalance. This dataset is publicly available [35]. Figure 3 shows samples of the COVIDx CXR-4 dataset.

V. EXPERIMENTAL SETUP

A. Transfer Learning as Image Embedding Generator

The dataset utilized in this study, COVIDx CXR-4, lacks sufficient data to train a deep neural network effectively using CNNs from scratch. Therefore, this study adopted the transfer learning (TL) approach to prepare the dataset for the proposed method. TL is a robust technique within machine learning that alleviates the computational burden and extensive data requirements associated with training CNNs from the ground up.

Here, the primary goal of TL was to transfer knowledge by using pre-trained models as an embedding function (or, more simply, feature extractors). These models, initially trained and optimized on extensive datasets such as ImageNet, had their final fully-connected layers removed, and the remaining network layers were frozen. This repurposed the networks as fixed feature extractors for the COVIDx CXR-4 dataset, effectively harnessing their pre-established computational intelligence for new data applications.

In this study, three different pre-trained models were utilized: EfficientNetB0 [36], BigTransfer [37], and Vision Transformer [38]. These models required an input image size of 224x224 pixels. Moreover, the output embedding (feature) vectors were standardized to 256 dimensions per image across all models. Utilizing an assortment of pre-trained models, including both CNNs and transformers, the study sought to minimize the impact of any individual model’s initial training on the overall outcomes.

B. Base model configuration

The embedding vectors (feature representations) extracted from the pre-trained models served as inputs for the base model. In this study, the base model is built using neural networks to perform binary classification. Considering the three different UQ techniques employed (MCD, Ensemble, and EMCD), the following configurations for the base model were devised and implemented:

1) *A Neural Network with MCD*: Here, a fully connected layers with an output layer equipped with a softmax function is employed. To determine the optimal architecture, the dataset was first split into training and testing sets using a 70/30 ratio. The training set was used to train the models, while the test set was reserved for evaluating their performance. Various architectures were explored by employing Keras Tuner’s Hyperband algorithm. Keras Tuner, a library built on top of TensorFlow and Keras, automates the hyperparameter tuning process. Hyperband, an advanced tuning algorithm, dynamically allocates resources to train multiple models, stopping those that underperform early. The search space included variations in the number of hidden layers, ranging from one to four, and the number of neurons per layer, ranging from 16 to 512. Given the imbalanced nature of the dataset, class weights were computed to ensure balanced learning across classes. These weights were incorporated during the training process to prevent bias towards the majority class. The best-performing architecture was selected as the optimal base model for evaluating the proposed method. Additionally, MCD was employed during the prediction phase to estimate the model’s uncertainty, which was crucial for the subsequent stages of the study. In this study, the number of iterations for MCD was set to 100.

In this study, three different pre-trained models were used, resulting in three sets of embedding vectors. For each set, a base model with its optimal architecture was determined. Table S1 in the Supplementary material summarizes the optimal architecture for each of the pre-trained models.

2) *An Ensemble of Neural Networks*: In this setting, the base model configuration leverages an ensemble approach. Thus, instead of relying on a single neural network, an ensemble of 30 distinct neural networks was employed. For each model in the ensemble, a neural network was built with a random number of hidden layers (ranging from one to four) and neurons per layer (ranging from 16 to 512) employing a softmax in the output layer. Similarly, class weights were utilized to address data imbalance for each neural network in the ensemble.

Table S2 in the Supplementary material provides a summary of the architectures for each model within the ensemble across the different pre-trained models.

3) *An Ensemble of Neural Networks with MCD*: This setting integrates MCD with an ensemble of neural networks. The purpose of this configuration is to observe how the introduction of dropout during inference affects uncertainty estimation and model robustness. This approach ensures a direct comparison with the previous ensemble setup by using the same ensemble model configuration as the prior setting, with the addition of MCD during the inference phase.

C. Meta-model configuration

The meta-model is designed as a neural network, and its optimal architecture is determined using the Keras Tuner’s Hyperband algorithm. This method, similar to that employed for the single neural network with the MCD base model, efficiently explores the hyperparameter space to identify the most effective architecture. The search space for the meta-model includes variations in the number of hidden layers, ranging from one to four, and the number of neurons per layer, ranging from 16 to 512, allowing the model to adapt to the complexities of the data. Class weights are again utilized to address data imbalance, maintaining fairness in the learning process.

For the meta-model dataset generation, the confidence threshold is a crucial parameter that impacts the labeling of the data. In this study, five different thresholds were used: 0.05, 0.1, 0.2, 0.3, and 0.4. These thresholds determine the cut-off points for labeling predictions as confident or not, which in turn affects the training and performance of the meta-model. By experimenting with these different thresholds, the study aims to identify the optimal level at which the model can reliably distinguish between confident and uncertain predictions.

VI. RESULTS AND DISCUSSION

This section delves into the empirical outcomes derived from the application of the proposed method:

- Initially, the analysis commences with a focus on a selected confidence threshold of 0.1, evaluating the performance across three distinct UQ settings: MCD, Ensemble, and EMCD. This section discusses their respective contributions to enhancing trust-informed decision-making. Additionally, this examination is broadened to include a discussion about the effects of various pre-trained models on the models’ performance, providing a

deeper understanding of how foundational architectures influence model reliability.

- Subsequently, the discourse broadens to include a comparative analysis across a spectrum of confidence thresholds, ranging from 0.05 to 0.4. This section aims to delineate how varying confidence levels influence the model’s accuracy and the efficacy of trust-informed decision-making, providing more insights into the model’s robustness.
- The final section investigates the integration of PE alongside image embeddings as inputs to the meta-models. This exploration is aimed at discerning the impact of such integrations on the overall efficacy and accuracy of the meta-model, thereby shedding light on the potential enhancements introduced by combining these inputs.

A. Results and discussion at Confidence Threshold 0.1:

The performance evaluation process begins with partitioning the dataset into training and testing sets through stratified sampling based on the target variable. This ensures that both sets maintain a similar distribution of classes. While evaluating a model on a single test set might provide an initial performance snapshot, it does not guarantee reproducible results across different data splits. This is because each random split could present the model with different distributions of data. When a model is trained on a specific training set, it learns patterns based on the distribution of that set. Similarly, the testing set used for evaluation will also have its unique distribution. Therefore, repeating the process with different splits can yield varying results, highlighting the non-reproducibility of single evaluations.

To address this variability and better gauge the model’s generalization capabilities, the training and evaluation process is repeated 30 times. For each iteration, the dataset is randomly split into training and testing sets, with a test size randomly chosen between [20%- 40%] of the data. This repetitive approach ensures that the model is exposed to various data distributions, enable evaluation of the model’s ability to generalize across various potential data distributions.

The evaluation metrics in this study are twofold. For the base model and meta-model, metrics include the F1 score and the Area Under the Curve (AUC). The F1 score and AUC are particularly suited for this study due to the imbalanced nature of the dataset.

Table II summarizes the base model performance across three UQ settings as well as pre-trained models. The evaluation of base model performance across different UQ settings reveals distinct patterns in classification effectiveness. The Ensemble setting, which utilizes 30 ANNs with varying architectures, generally improves F1 scores compared to MCD, reflecting enhanced precision and recall due to the collective decision-making of multiple networks. However, this setting shows a tendency for lower AUC values, likely due to the inclusion of networks that vary in strength, potentially affecting overall class discrimination. The EMCD setting, which applies dropout during inference across the ensemble, exhibits performance metrics similar to the Ensemble setting. This similarity is logical, as EMCD combines the architectural diversity

TABLE II: Summary of base models' performance across various pre-trained models

Pre-trained Model	UQ	F1 score	AUC
BiT	MCD	$\%85.7497 \pm 0.3985$	$\%92.5964 \pm 0.3318$
BiT	Ensemble	$\%86.5468 \pm 0.3755$	$\%83.1988 \pm 0.4327$
BiT	EMCD	$\%85.7741 \pm 0.3639$	$\%82.6929 \pm 0.6457$
EfficientNetB0	MCD	$\%84.4497 \pm 0.4569$	$\%91.5801 \pm 0.2291$
EfficientNetB0	Ensemble	$\%85.3409 \pm 0.2922$	$\%81.9711 \pm 0.3356$
EfficientNetB0	EMCD	$\%84.2926 \pm 0.4880$	$\%81.1628 \pm 0.7131$
ViT	MCD	$\%86.9507 \pm 0.4568$	$\%94.2096 \pm 0.3157$
ViT	Ensemble	$\%88.0198 \pm 0.2486$	$\%84.8285 \pm 0.2681$
ViT	EMCD	$\%87.0202 \pm 0.4014$	$\%84.1501 \pm 0.5857$

TABLE III: Summary of meta-models' performance across various pre-trained models at the confidence threshold 0.1

Model	UQ	F1 score	AUC
BiT	MCD	$\%96.6539 \pm 0.3515$	$\%99.5043 \pm 0.0949$
BiT	Ensemble	$\%96.5189 \pm 0.3838$	$\%99.5790 \pm 0.0712$
BiT	EMCD	$\%96.4965 \pm 0.4470$	$\%99.4579 \pm 0.1353$
EfficientNetB0	MCD	$\%96.3704 \pm 0.4546$	$\%99.4674 \pm 0.1265$
EfficientNetB0	Ensemble	$\%95.7363 \pm 0.5624$	$\%99.4962 \pm 0.1177$
EfficientNetB0	EMCD	$\%96.0171 \pm 0.5652$	$\%99.4466 \pm 0.1381$
ViT	MCD	$\%97.4823 \pm 0.3232$	$\%99.6293 \pm 0.1102$
ViT	Ensemble	$\%97.6332 \pm 0.2767$	$\%99.7606 \pm 0.0379$
ViT	EMCD	$\%97.4426 \pm 0.3090$	$\%99.6196 \pm 0.0865$

of the ensemble with dropout at inference, maintaining the ensemble's overall classification characteristics. A higher AUC for MCD suggests that fine-tuning the single neural network contributed to better class discrimination, as evidenced by the AUC. In contrast, the Ensemble and EMCD settings improve precision and recall (reflected in higher F1 scores) but introduce variability due to the random architectures, which may affect the overall AUC. Results across pre-trained models highlight ViT's strength in leveraging its architectural design to enhance classification accuracy and discrimination. The BiT model also shows competitive performance, particularly in F1 scores, reflecting its capacity to balance precision and recall effectively. However, BiT's AUC values are slightly lower than those of ViT, indicating some limitations in its ability to separate classes with the same level of distinction. EfficientNetB0 exhibits the lowest performance among the pre-trained models, with both F1 scores and AUC values trailing behind ViT and BiT. This suggests that while EfficientNetB0 can achieve reasonable classification results, it may not capture the nuances of the data as effectively as the other models. This performance gap behind ViT and BiT could be attributed to the architecture of EfficientNetB0, which is a lighter model with significantly fewer parameters compared to ViT and BiT. These findings suggest that selecting ViT with MCD offers the finest balance of accuracy and robustness, making it the preferred choice for the problem addressed in this study.

Similarly, Table III illustrates the meta-model performance across three UQ settings as well as pre-trained models. It is worth noting that the meta-model across all pre-trained models and UQ settings is a single neural network fine-tuned using the Keras Tuner. The influence of the UQ settings lies in the additional input variable, Prediction Entropy (PE), which is derived from the uncertainty estimation of each UQ method, as well as the target variable defined by Eq. 1, which also depends on PE. Overall, all models exhibit high AUC values, consistently surpassing 99%, indicating a strong ability to

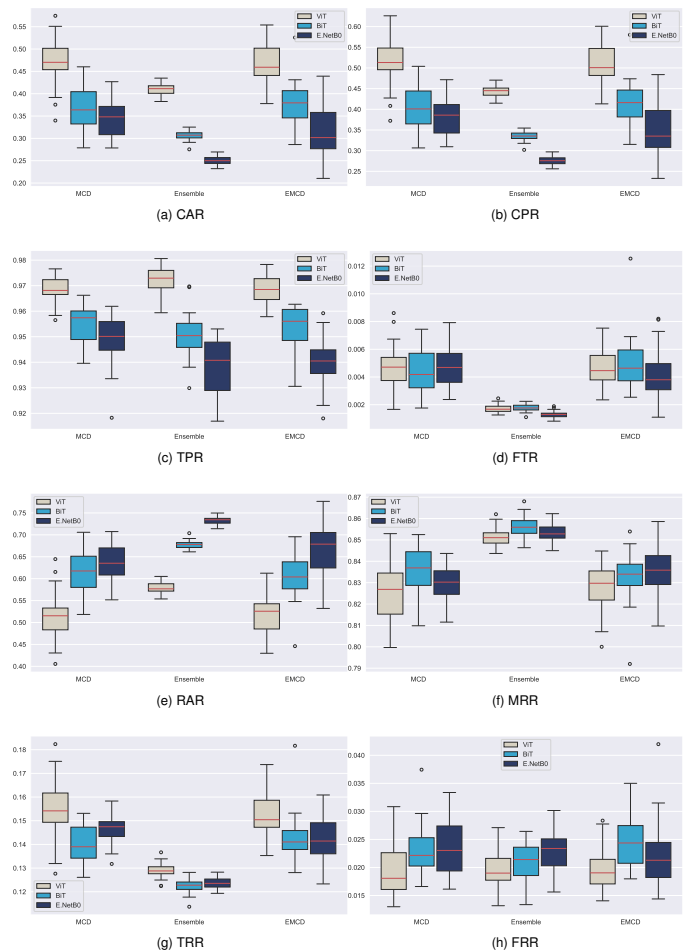


Fig. 4: Comparison of Uncertainty-Informed Criteria Across Pre-trained Models Using different UQ Methods at Confidence Threshold 0.1

discriminate between classes across the UQ settings and pre-trained models. Notably, the ViT models achieved the highest F1 scores and AUC values. In comparison, the EfficientNetB0 models show slightly lower F1 scores but still maintain high AUC values, reflecting reliable classification performance with minor variations across different UQ methods. The BiT models perform consistently across all UQ settings, although they exhibit slightly lower F1 scores and AUC values compared to the ViT models, suggesting that ViT models may be better suited for the task at this confidence threshold. Among the UQ methods, the Ensemble method provides the best performance in terms of AUC, particularly with the ViT models. The MCD method also performs competitively, especially with the ViT models, though it falls slightly behind the Ensemble method in terms of F1 scores. Meanwhile, the EMCD method, while maintaining high AUC values, shows slightly lower F1 scores, indicating that it may not balance precision and recall as effectively as the other methods at this specific threshold.

Having established that both the base and meta-models individually exhibit strong performance, it is essential to evaluate the effectiveness of the overall framework when considering the combined outputs of both models. This comprehensive

TABLE IV: Comparative performance of proposed method: Summary of trust-informed criteria across various pre-trained models at the confidence threshold 0.1.

Pretrained	UQ Setting	CAR	CPR	TPR	FTR	RAR	MRR	TRR	FRR
BiT	MCD	% 37.064 ± 4.997	% 40.731 ± 5.441	% 95.485 ± 0.768	% 0.440 ± 0.148	% 61.201 ± 5.090	% 83.625 ± 1.055	% 14.079 ± 0.842	% 2.297 ± 0.455
BiT	Ensemble	% 30.663 ± 1.074	% 33.502 ± 1.153	% 95.039 ± 0.844	% 0.178 ± 0.025	% 67.739 ± 1.005	% 85.633 ± 0.483	% 12.249 ± 0.306	% 2.119 ± 0.350
BiT	EMCD	% 37.865 ± 4.583	% 41.617 ± 5.036	% 95.372 ± 0.872	% 0.490 ± 0.195	% 60.299 ± 4.795	% 83.328 ± 1.079	% 14.214 ± 0.956	% 2.459 ± 0.442
E.NetB0	MCD	% 34.319 ± 3.841	% 38.055 ± 4.215	% 94.918 ± 0.922	% 0.476 ± 0.151	% 63.850 ± 3.973	% 82.980 ± 0.855	% 14.681 ± 0.641	% 2.339 ± 0.468
E.NetB0	Ensemble	% 25.071 ± 1.021	% 27.607 ± 1.100	% 93.831 ± 1.079	% 0.129 ± 0.025	% 73.284 ± 0.954	% 85.335 ± 0.450	% 12.362 ± 0.212	% 2.303 ± 0.376
E.NetB0	EMCD	% 31.305 ± 5.702	% 34.733 ± 6.272	% 94.002 ± 0.862	% 0.416 ± 0.184	% 66.717 ± 5.954	% 83.502 ± 1.130	% 14.272 ± 0.896	% 2.226 ± 0.556
ViT	MCD	% 46.845 ± 5.484	% 51.126 ± 5.940	% 96.907 ± 0.511	% 0.462 ± 0.165	% 51.665 ± 5.613	% 82.605 ± 1.471	% 15.452 ± 1.255	% 1.943 ± 0.495
ViT	Ensemble	% 40.995 ± 1.171	% 44.378 ± 1.248	% 97.222 ± 0.487	% 0.173 ± 0.029	% 57.834 ± 1.167	% 85.156 ± 0.434	% 12.885 ± 0.308	% 1.959 ± 0.363
ViT	EMCD	% 46.672 ± 4.445	% 50.901 ± 4.767	% 96.861 ± 0.595	% 0.467 ± 0.134	% 51.816 ± 4.568	% 82.797 ± 1.055	% 15.228 ± 0.913	% 1.975 ± 0.382

performance assessment is presented in Table IV, which details the proposed metrics discussed in Section III-C.

To start, let’s first examine the results of the ViT model with MCD, providing an interpretation of each metric. For the ViT model using the MCD setting, the CAR is 46.85%. This indicates that 46.85% of the total outcomes were both correct and made with high confidence (i.e., trustworthy). This metric suggests that a significant portion of the model’s predictions can be trusted without further verification.

The CPR is about 51.13%, suggesting that 51.16% of correctly predicted by the base model flagged as trustworthy by meta-model. This suggests that while almost half of the correct predictions made by the base model were identified as trustworthy by the meta-model, the other half were not flagged as trustworthy. This could be due to either the miscalibration of the base model (i.e., correct predictions with a predictive entropy greater than the confidence threshold) or errors from the meta-model.

The TPR is about 96.90%, implying among the instances the model flagged as trustworthy, 96.70% were indeed trustworthy (or in other words correct and confidently made). In other words, the model’s trustworthiness flagging mechanism is highly reliable, as nearly all of the predictions marked as trustworthy were both accurate and confident.

The FTR 0.462% indicates that 0.46% of the total outcomes erroneously flagged incorrect predictions as trustworthy. While this error rate is quite low, it underscores the potential for further reducing the chances of misplaced trust in incorrect outcomes.

The RAR is around 51.67%, meaning that over half of the model’s predictions were flagged as untrustworthy (i.e., either uncertainly correct, uncertainly incorrect, or confidently incorrect). This high percentage leading to a significant review burden.

The MRR is 82.60%, indicating that 82.60% of the instances flagged as untrustworthy for review (in other words, 82.60% of RAR) are due to the base model’s miscalibration, where correct predictions with low confidence (or high uncertainty) are flagged as untrustworthy and require further review. This high percentage indicates that the base model struggles to be confident in its correct predictions.

The TRR is relatively low at 15.45%, showing that 15.45% of RAR were correctly flagged as untrustworthy due to incorrect predictions. The FRR is low at around 1.94%, indicating that a small percentage of RAR were mistakenly flagged as untrustworthy due to meta-model errors (flag confidently correct prediction as untrustworthy by meta-model error). This is a positive outcome, as it suggests the model rarely

creates unnecessary reviews by incorrectly doubting its correct predictions.

Across all UQ settings, it is apparent that there exists a notable relationship between the CAR and RAR. As CAR increases (from 25.07% with EfficientNetB0 Ensemble to 46.85% with ViT MCD), there is a concomitant decrease in RAR (from 73.28% to 51.67%). This trend aligns with the intuitive understanding that enhancing model performance inherently reduces the need for additional review, thereby diminishing the review burden.

The MCD setting, with a higher AUC score, excels in distinguishing correct predictions with confidence. This is reflected in its relatively higher CAR and CPR values. On the other hand, the Ensemble setting, despite having almost similar AUC scores to EMCD, excels with the lowest FTR. This means that the Ensemble setting by aggregating predictions from multiple models enhances the F1 score, thereby reducing FTR. However, Ensemble’s lower CAR and CPR, despite its high F1 score, suggest that while it can identify correct predictions its confidence in these predictions is not as well-calibrated due to the variability in predictions introduced by the ensemble approach. This variability in predictions observed in the Ensemble setting is also reflected in the higher RAR and MRR. Conversely, MCD, by incorporating dropout during inference, effectively captures uncertainty and enhances the model’s ability to discern when it should be confident in its predictions. However, the slightly higher FTR compared to Ensemble suggests that MCD may occasionally place trust in incorrect predictions. EMCD, by introducing stochasticity during the inference phase of the ensemble, provides improved uncertainty estimations. This approach achieves an AUC comparable to that of Ensemble while attaining higher CAR and CPR, along with lower RAR and MRR, demonstrating performance closely rivaling that of MCD. However, it is important to note that while EMCD and MCD exhibit similar performance, EMCD is considerably more computationally demanding due to the necessity of maintaining an ensemble of models (30 in this study), as opposed to the single fine-tuned model employed in MCD. These findings suggest that the MCD approach may offer a more reliable and stable solution, striking an optimal balance between performance efficiency and computational complexity.

Across the evaluated pre-trained models, ViT consistently demonstrates superior performance compared to BiT and EfficientNetB0, particularly in its ability to generate confident and accurate predictions. Generally, EfficientNetB0 lags behind ViT and BiT, showing lower CAR and higher FTR values. This suggests that while EfficientNetB0 can achieve reasonable

classification results, it may not capture the nuances of the data as effectively as the other models. These findings underscore the critical role of the pre-trained model in effectively capturing prediction uncertainty and facilitating trust-informed decision-making.

B. Ablation study part One: Influence of Variable Confidence Thresholds

To further investigate the impact of the confidence threshold (τ) on the performance of the meta-model, an ablation analysis was conducted. This analysis involved systematically varying τ from 0.05 to 0.4 and observing the changes in the model’s ability to distinguish between trustworthy and untrustworthy predictions, illustrated by Figure 5 and Table Supplementary S.V. The error-based performance metrics, such as F1 score and AUC, of the meta-model at each confidence threshold are presented in Supplementary Table S.IV. While all meta-models across various confidence thresholds demonstrate strong performance, the focus of this section is to examine the effect of the confidence threshold on trust-informed decision-making.

It is worth recalling that a PE value closer to 1 indicates lower confidence (higher uncertainty), while a PE value closer to 0 reflects higher confidence (lower uncertainty). Accordingly, as the τ increases, the model becomes less conservative—meaning it is more permissive about what it labels as trustworthy. When the threshold is low (close to zero), the model is stricter, only labeling correct predictions as trustworthy if they have very low entropy, thus demonstrating high confidence. Thus a clear upward trend in the Mean CAR is observed across all pre-trained models and UQ settings. This trend indicates that as the threshold increases, the model becomes more willing to label a greater number of correct predictions as trustworthy, and similarly, CPR also shows an upward trajectory with increasing thresholds.

As the confidence threshold increases, TPR initially rises, reaches a peak, and then either stabilizes or decreases. At lower thresholds (e.g., 0.05), the model is more conservative, labeling only predictions with very low uncertainty as trustworthy, which limits the number of predictions flagged as trustworthy. As the confidence threshold increases, the model becomes less conservative, allowing more predictions to be flagged as trustworthy, thereby initially improving TPR as more correct predictions are included. However, beyond a certain point, the model’s selectivity decreases, leading to a potential increase in incorrect predictions being erroneously flagged as trustworthy as mirrored by the upward trend in FTR. This suggests that while increasing the confidence threshold can initially improve the model’s trustworthiness in its correct predictions, it may also lead to a higher rate of false trust in incorrect predictions.

As the τ increases, Mean RAR exhibit a clear downward trend across all models and UQ settings. The decline in RAR as τ increases indicates that fewer predictions are being flagged as uncertain and sent for review. This is likely because as the model becomes more lenient (by allowing predictions with slightly higher entropy to be considered trustworthy), it flags fewer predictions as requiring review, reducing the review

burden. Also, the inverse relationship between CAR and RAR is intuitive: as the model becomes better at identifying trustworthy predictions (higher CAR), the need for further human review diminishes (lower RAR).

Simultaneously, the decrease in MRR with an increasing confidence threshold indicates that the proportion of review cases attributed to base model miscalibration is also reducing. This suggests that as the confidence threshold rises, the instances where the base model is correct but uncertain (leading to unnecessary review) become less frequent. This reduction aligns with the decrease in RAR, reinforcing the idea that a higher confidence threshold not only reduces the total number of reviews but also leads to fewer correctly predicted instances being flagged for review.

As the τ increases, FRR and TRR exhibit an upward trend. At first glance, this may seem counterintuitive, particularly given the simultaneous decrease in the RAR, which might lead to the expectation that FRR and TRR would also decrease. The explanation lies in the interaction between the changing threshold and the total uncertain predictions (TUP). As τ increases, the model becomes more permissive, leading to fewer predictions being flagged as untrustworthy, which decreases the TUP (Eq. 15). The correctness of a prediction, as determined by comparing the predicted labels to actual labels, remains independent of the confidence threshold. Therefore, the absolute number of incorrect predictions does not change. The increase in TRR as τ increases can be attributed to the decrease in TUP. As fewer predictions are labeled as untrustworthy, the relative proportion of incorrect predictions (which remain constant in absolute terms) becomes larger. Similarly, the increase in FRR with rising τ is due to the shrinking pool of TUP, combined with the possibility of increasing meta-model errors, as indicated by the upward trend in FTR.

C. Ablation Study part Two: Evaluating the Integration of PE and Image Embeddings

In this ablation study, the impact of incorporating PE as an input to the meta-model was examined. The meta-model was trained under two conditions: one in which PE was included alongside the feature representations from the pre-trained model, and another in which only the feature representations were used as input. This approach allows for an assessment of the significance of PE in enhancing the meta-model’s performance.

Table V presents the error-based performance results of the meta-model excluding PE at $\tau=0.1$. Supplementary Table S.IV provides a summary of the error-based performance results, comparing models with and without PE across various τ values. Figure 6 illustrates the performance comparison of the meta-model at $\tau=0.1$, while Supplementary Figures S.1 to S.4 display the error-based performance comparisons at τ values of 0.05, 0.2, 0.3, and 0.4, respectively.

The comparison between meta-models that include PE as input and those that exclude it reveals a consistent trend across both F1 scores and AUC values. Meta-models that incorporate PE as part of their input tend to achieve higher F1 scores, as

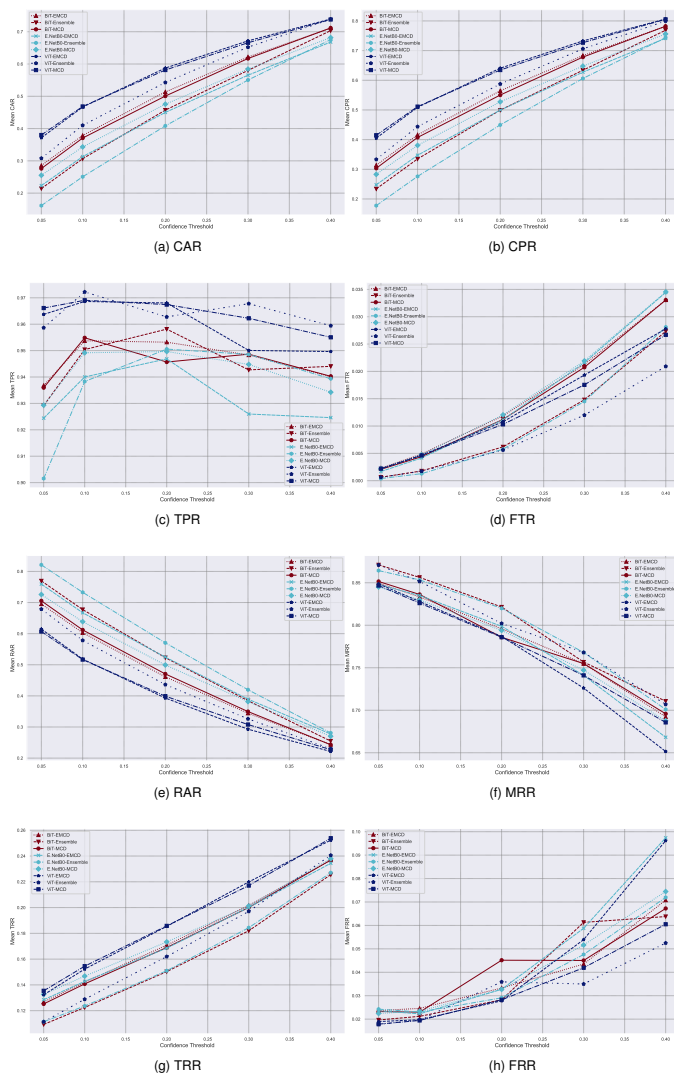


Fig. 5: Trend Analysis of Uncertainty-Informed Criteria Across Various Pre-trained Models at Incremental Confidence Thresholds from 0.05 to 0.4.

TABLE V: Performance Summary of Meta-Models Across Pre-trained Models, Excluding PE as Input at Confidence Threshold 0.1

Model	UQ	F1 score	AUC
BiT	MCD	%91.9709 \pm 1.0608	%97.9825 \pm 0.5543
BiT	Ensemble	%92.8740 \pm 0.3631	%98.5293 \pm 0.1335
BiT	EMCD	%91.7319 \pm 0.9978	%97.8230 \pm 0.5589
EfficientNetB0	MCD	%91.1689 \pm 1.1750	%97.6144 \pm 0.7021
EfficientNetB0	Ensemble	%92.2438 \pm 0.4211	%98.4108 \pm 0.1596
EfficientNetB0	EMCD	%90.6849 \pm 1.1943	%97.4026 \pm 0.7684
ViT	MCD	%91.0680 \pm 1.1215	%97.4382 \pm 0.5998
ViT	Ensemble	%92.5409 \pm 0.4308	%98.2399 \pm 0.1796
ViT	EMCD	%90.9633 \pm 1.0366	%97.3828 \pm 0.5639

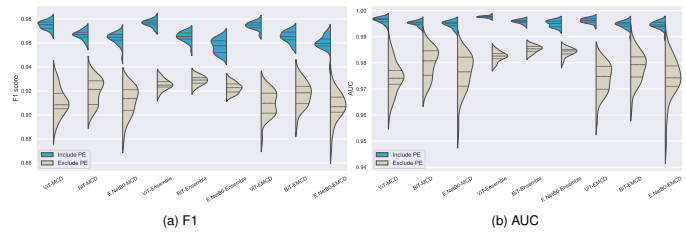


Fig. 6: Comparative Performance of Meta-Models With and Without PE as Input at Confidence Threshold 0.1.

well as AUC, across all pre-trained models and UQ settings. This suggests that incorporating PE enables the meta-model to more effectively differentiate between trustworthy and untrustworthy predictions. The additional information provided by PE, which quantifies the uncertainty of predictions, allows the model to make more informed decisions. The underlying reason for these improvements is that PE provides the meta-model with crucial contextual information about the certainty of predictions. Without PE, the meta-model relies solely on feature representations, which may not fully capture the uncertainty associated with each prediction. By incorporating PE, the model can adjust its predictions based on its confidence, leading to more accurate and reliable performance. This is particularly valuable in settings where the cost of incorrect predictions is high, and it is essential to identify instances where the model is uncertain.

Improvement in the meta-model’s performance also enhances trust-informed decision-making. Table VI presents the results of the proposed trust-informed metrics excluding PE at $\tau=0.1$. Supplementary Table S.V provides a summary of these results, comparing models with and without PE across various τ values. Figure 7 illustrates the performance comparison of the proposed metrics at $\tau=0.1$, while Supplementary Figures S.5 to S.8 display the performance comparisons at τ values of 0.05, 0.2, 0.3, and 0.4, respectively.

The enhanced performance of the meta-model, as demonstrated in the presented results, translates into improved trust-informed decision-making. The improvement is reflected in the increase in CAR, indicating that the model is more accurate when making confident predictions. Similarly, the improvement in CPR with the inclusion of PE indicates that when the model is correct in its predictions, it is more likely to be confident. This is a crucial factor in trust-informed decision-making, as it implies that the meta-model is not only making accurate predictions but is also more reliable when it asserts trust. The enhanced performance of the meta-model is more significant in TPR suggesting that incorporating PE allows the meta-models to better discern between correct predictions that are genuinely confident and those that are not. The increase in CPR and TPR across different settings further supports the notion that PE helps the model to align its confidence with its accuracy, making the overall decision-making process more trustworthy.

Including PE appears to lower the FTR across various pre-trained models and UQ settings. This result is expected

because FTR reflects instances where both the base model and the meta-model make errors. By enhancing the meta-model’s performance with the inclusion of PE (as reflected in Figure 6, the likelihood of errors by the meta-model decreases. As a result, the overall incidence of compounded errors—where both models fail simultaneously—decreases.

The RAR, which measures the proportion of predictions flagged as untrustworthy, appears relatively unaffected by the inclusion or exclusion of PE across different settings. This stability in RAR can be attributed to the balancing effect within the total uncertain predictions (TUP) metric. On one hand, the inclusion of PE enhances the meta-model’s ability to correctly identify trustworthy (TT) versus untrustworthy (TU) predictions. This improvement should theoretically decrease the number of incorrect predictions flagged as untrustworthy (FU), which would reduce the TUP and, by extension, the RAR. On the other hand, the same improvement might also enhance the meta-model’s ability to correctly identify uncertainly correct predictions (TPTU, TNTU), which could increase these components of the TUP. As a result, the overall TUP might not change significantly.

The exclusion of PE appears to result in a slight decrease in MRR, particularly noticeable in ensemble settings. This decrease, however, does not necessarily indicate an actual improvement. Rather, it may reflect the meta-model’s reduced ability to accurately discern between trustworthy and untrustworthy predictions. MRR is calculated based on how well the model identifies instances where the base model is either confidently incorrect (FPTT, FNTT) or uncertainly correct (TPTU, TNTU). When PE is excluded, the meta-model’s performance decreases, making it less effective in correctly identifying these instances. As a result, the MRR metric may decrease, not because the base model is better calibrated, but because the meta-model is less capable of capturing true instances of miscalibration. Therefore, the slight decrease in MRR when excluding PE suggests a reduction in the meta-model’s effectiveness in highlighting the base model’s calibration issues, rather than an actual improvement in calibration.

The inclusion of PE results does not significantly impact the TRR. TRR measures the proportion of instances where the model makes an incorrect prediction and correctly flags this prediction as untrustworthy. The observed pattern where including PE does not significantly alter TRR suggests that PE might not be adding much value in terms of enhancing the meta-model’s ability to recognize these erroneous predictions. This could be because the TRR is heavily dependent on the base model’s performance since it is based on the incorrect predictions made by the base model. If the base model’s error patterns are consistent and not highly correlated with PE, the meta-model may find limited use for PE in distinguishing trustworthy from untrustworthy errors. This suggests that while PE can be valuable in other contexts, such as improving other trust-related metrics like TPR and FTR, its role in enhancing TRR specifically is limited in this setup.

On the other hand, the inclusion of PE in the meta-model shows a distinct impact on the FRR. FRR is formulated as the proportion of correct predictions that are incorrectly flagged

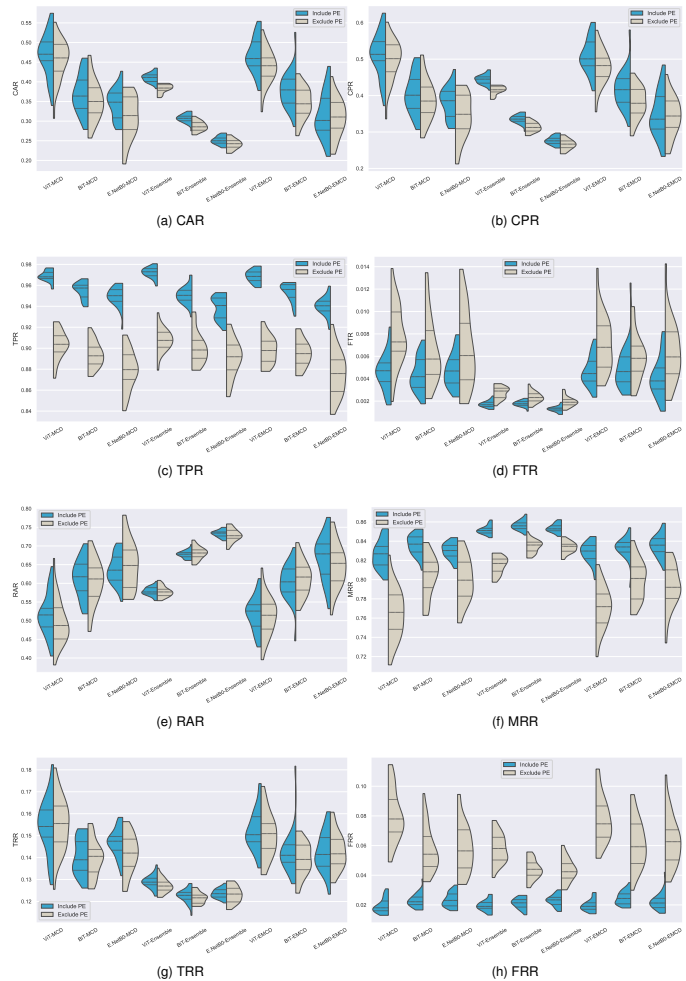


Fig. 7: Comparison of Uncertainty-Informed Criteria Across Pre-trained Models at a Confidence Threshold of 0.1, With and Without PE as Input.

as untrustworthy due to the meta-model’s error. It is evident that including PE leads to a noticeable decrease in FRR across most pre-trained models and UQ settings. The improvement in the meta-model’s performance ensures that fewer correct predictions are mistakenly flagged for review. In conclusion, the inclusion of PE significantly enhances the meta-model’s ability to discern between trustworthy and untrustworthy predictions, leading to a more reliable and efficient trust-informed decision-making process.

VII. CONCLUSION

The application of AI in high-stakes fields such as medical diagnosis holds immense potential for improving outcomes, yet widespread adoption is hindered by a lack of trust, primarily due to variations in model performance. A key challenge lies in addressing confidently incorrect predictions—cases where the model makes an incorrect prediction with high confidence—alongside the more straightforward detection of uncertain predictions. This research addresses this critical issue by proposing a framework that not only identifies uncertain

TABLE VI: Summary of trust-informed criteria across various pre-trained models, Excluding PE as Input at the confidence threshold 0.1.

Pretrained	UQ Setting	CAR	CPR	TPR	FTR	RAR	MRR	TRR	FRR
BiT	MCD	% 35.361 ± 5.106	% 38.868 ± 5.567	% 89.421 ± 1.189	% 0.648 ± 0.292	% 60.415 ± 5.986	% 80.351 ± 2.156	% 13.961 ± 0.833	% 5.688 ± 1.494
BiT	Ensemble	% 28.736 ± 1.216	% 31.406 ± 1.315	% 90.052 ± 1.560	% 0.232 ± 0.049	% 68.072 ± 1.639	% 83.458 ± 0.660	% 12.153 ± 0.258	% 4.389 ± 0.645
BiT	EMCD	% 34.646 ± 3.880	% 38.111 ± 4.262	% 89.494 ± 1.259	% 0.597 ± 0.209	% 61.264 ± 4.520	% 79.956 ± 2.052	% 13.918 ± 0.745	% 6.126 ± 1.589
E.NetB0	MCD	% 31.121 ± 5.406	% 34.487 ± 5.981	% 87.898 ± 1.831	% 0.661 ± 0.335	% 64.552 ± 6.378	% 80.051 ± 2.315	% 14.181 ± 0.884	% 5.768 ± 1.616
E.NetB0	Ensemble	% 24.154 ± 1.270	% 26.592 ± 1.391	% 89.103 ± 1.792	% 0.194 ± 0.044	% 72.870 ± 1.725	% 83.345 ± 0.584	% 12.323 ± 0.375	% 4.331 ± 0.772
E.NetB0	EMCD	% 30.786 ± 4.908	% 34.151 ± 5.407	% 87.659 ± 2.128	% 0.636 ± 0.269	% 64.824 ± 5.882	% 79.386 ± 2.257	% 14.309 ± 0.827	% 6.305 ± 1.662
ViT	MCD	% 45.522 ± 5.137	% 49.690 ± 5.573	% 90.339 ± 1.324	% 0.781 ± 0.266	% 49.571 ± 5.952	% 76.462 ± 2.582	% 15.491 ± 1.222	% 8.047 ± 1.693
ViT	Ensemble	% 38.329 ± 1.072	% 41.489 ± 1.143	% 90.771 ± 1.096	% 0.272 ± 0.053	% 57.765 ± 1.378	% 81.480 ± 0.884	% 12.720 ± 0.317	% 5.800 ± 0.948
ViT	EMCD	% 43.850 ± 4.403	% 47.841 ± 4.764	% 89.831 ± 1.294	% 0.704 ± 0.248	% 51.146 ± 5.269	% 77.165 ± 2.199	% 15.042 ± 1.029	% 7.793 ± 1.543

predictions but also accurately flags confidently incorrect predictions, thereby enhancing trust in ML models. The proposed architecture consists of two levels: a base model (Level 0) that provides predictions and generates a PE measure, and a meta-model (Level 1) that leverages both the feature representations and PE from the base model to learn and predict a trust flag. This trust flag, combined with the predicted class, provides a final output indicating both the class prediction and the associated confidence level, categorized as either trustworthy or untrustworthy.

The results of this study indicate that the MCD setting consistently offers a reliable performance baseline across all pre-trained models, serving as a stable foundation for trust-informed decision-making. While the Ensemble setting enhances precision and recall, as evidenced by improved F1 scores, it can introduce variability that impacts the AUC. The EMCD setting, which combines the strengths of MCD and Ensemble strategies, achieves performance metrics comparable to MCD, effectively balancing robustness and variability while maintaining high reliability across all models. Among the pre-trained models evaluated, the ViT emerges as the top performer across all UQ settings, demonstrating superior capability in generating confident and accurate predictions. The BiT model also shows strong performance, particularly under the MCD and EMCD settings, highlighting its reliability in various scenarios.

Moreover, the selection of an appropriate confidence threshold is crucial. Lower confidence thresholds, which increase the number of predictions flagged for review, may be appropriate for scenarios where the stakes are high, such as critical medical diagnoses. Furthermore, the inclusion of PE as an input to the meta-model significantly enhances its performance, resulting in more accurate identification of trustworthy predictions. This enhancement underscores the importance of PE in refining the trustworthiness of ML models and ensuring more reliable decision-making processes in high-stakes environments. Future research is directed toward exploring the enhancement of base model calibration by leveraging the proposed trust-informed confusion matrix. Such advancements have the potential to reduce the RAR and MRR, while simultaneously improving the CAR, CPR, and TPR.

REFERENCES

- [1] C. Jin, W. Chen, Y. Cao, Z. Xu, Z. Tan, X. Zhang, L. Deng, C. Zheng, J. Zhou, H. Shi *et al.*, "Development and evaluation of an artificial intelligence system for covid-19 diagnosis," *Nature communications*, vol. 11, no. 1, p. 5088, 2020.
- [2] V. K. Bürger, J. Amann, C. K. Bui, J. Fehr, and V. I. Madai, "The unmet promise of trustworthy ai in healthcare: why we fail at clinical translation," *Frontiers in Digital Health*, vol. 6, p. 1279629, 2024.
- [3] M. Cheng, X. Li, and J. Xu, "Promoting healthcare workers' adoption intention of artificial-intelligence-assisted diagnosis and treatment: The chain mediation of social influence and human-computer trust," *International Journal of Environmental Research and Public Health*, vol. 19, no. 20, p. 13311, 2022.
- [4] J. Fehr, B. Citro, R. Malpani, C. Lippert, and V. I. Madai, "A trustworthy ai reality-check: the lack of transparency of artificial intelligence products in healthcare," *Frontiers in Digital Health*, vol. 6, p. 1267290, 2024.
- [5] M. Abdar, F. Pourpanah, S. Hussain, D. Rezazadegan, L. Liu, M. Ghavamzadeh, P. Fieguth, X. Cao, A. Khosravi, U. R. Acharya *et al.*, "A review of uncertainty quantification in deep learning: Techniques, applications and challenges," *Information fusion*, vol. 76, pp. 243–297, 2021.
- [6] Y. Gal and Z. Ghahramani, "Dropout as a bayesian approximation: Representing model uncertainty in deep learning," in *international conference on machine learning*. PMLR, 2016, pp. 1050–1059.
- [7] A. O. Aseeri, "Uncertainty-aware deep learning-based cardiac arrhythmias classification model of electrocardiogram signals," *Computers*, vol. 10, no. 6, p. 82, 2021.
- [8] D. Gamerman and H. F. Lopes, *Markov chain Monte Carlo: stochastic simulation for Bayesian inference*. Chapman and Hall/CRC, 2006.
- [9] A. Graves, "Practical variational inference for neural networks," *Advances in neural information processing systems*, vol. 24, 2011.
- [10] D. P. Kingma and M. Welling, "Auto-encoding variational bayes," *arXiv preprint arXiv:1312.6114*, 2013.
- [11] M. Fortunato, C. Blundell, and O. Vinyals, "Bayesian recurrent neural networks," *arXiv preprint arXiv:1704.02798*, 2017.
- [12] C. Martín Vicario, D. Rodríguez Salas, A. Maier, S. Hock, J. Kuramatsu, B. Kallmuenzer, F. Thamm, O. Taubmann, H. Ditt, S. Schwab *et al.*, "Uncertainty-aware deep learning for trustworthy prediction of long-term outcome after endovascular thrombectomy," *Scientific Reports*, vol. 14, no. 1, p. 5544, 2024.
- [13] Z. Senousy, M. M. Abdelsamea, M. M. Gaber, M. Abdar, U. R. Acharya, A. Khosravi, and S. Nahavandi, "Mcu: Multi-level context and uncertainty aware dynamic deep ensemble for breast cancer histology image classification," *IEEE Transactions on Biomedical Engineering*, vol. 69, no. 2, pp. 818–829, 2021.
- [14] G. Carneiro, L. Z. C. T. Pu, R. Singh, and A. Burt, "Deep learning uncertainty and confidence calibration for the five-class polyp classification from colonoscopy," *Medical image analysis*, vol. 62, p. 101653, 2020.
- [15] M. Habibpour, H. Gharoun, M. Mehdipour, A. Tajally, H. Asgharnejad, A. Shamsi, A. Khosravi, and S. Nahavandi, "Uncertainty-aware credit card fraud detection using deep learning," *Engineering Applications of Artificial Intelligence*, vol. 123, p. 106248, 2023.
- [16] P. Westermann and R. Evins, "Using bayesian deep learning approaches for uncertainty-aware building energy surrogate models," *Energy and AI*, vol. 3, p. 100039, 2021.
- [17] Y. Yao, T. Han, J. Yu, and M. Xie, "Uncertainty-aware deep learning for reliable health monitoring in safety-critical energy systems," *Energy*, vol. 291, p. 130419, 2024.
- [18] A. C. Teixeira, H. Yazdanpanah, A. Pezente, and M. Ghassemi, "Bayesian networks improve out-of-distribution calibration for agribusiness delinquency risk assessment," in *Proceedings of the Fourth ACM International Conference on AI in Finance*, 2023, pp. 244–252.
- [19] J. I. Aizpurua, V. M. Catterson, B. G. Stewart, S. D. McArthur, B. Lambert, and J. G. Cross, "Uncertainty-aware fusion of probabilistic classifiers for improved transformer diagnostics," *IEEE Transactions on*

- Systems, Man, and Cybernetics: Systems*, vol. 51, no. 1, pp. 621–633, 2018.
- [20] A. Shamsi, H. Asgharnezhad, S. S. Jokandan, A. Khosravi, P. M. Kebria, D. Nahavandi, S. Nahavandi, and D. Srinivasan, “An uncertainty-aware transfer learning-based framework for covid-19 diagnosis,” *IEEE transactions on neural networks and learning systems*, vol. 32, no. 4, pp. 1408–1417, 2021.
- [21] M. Habibpour, H. Gharoun, A. Tajally, A. Shamsi, H. Asgharnezhad, A. Khosravi, and S. Nahavandi, “An uncertainty-aware deep learning framework for defect detection in casting products,” *arXiv preprint arXiv:2107.11643*, 2021.
- [22] E. Aguilar, B. Nagarajan, and P. Radeva, “Uncertainty-aware selecting for an ensemble of deep food recognition models,” *Computers in Biology and Medicine*, vol. 146, p. 105645, 2022.
- [23] P. Tabarisaadi, A. Khosravi, S. Nahavandi, M. Shafie-Khah, and J. P. Catalão, “An optimized uncertainty-aware training framework for neural networks,” *IEEE transactions on neural networks and learning systems*, 2022.
- [24] X. Li, X. Liang, G. Luo, W. Wang, K. Wang, and S. Li, “Ultra: Uncertainty-aware label distribution learning for breast tumor cellularity assessment,” in *International Conference on Medical Image Computing and Computer-Assisted Intervention*. Springer, 2022, pp. 303–312.
- [25] A. Shamsi, H. Asgharnezhad, Z. Bouchani, K. Jahanian, M. Saberi, X. Wang, I. Razzak, R. Alizadehsani, A. Mohammadi, and H. Alinejad-Rokny, “A novel uncertainty-aware deep learning technique with an application on skin cancer diagnosis,” *Neural Computing and Applications*, vol. 35, no. 30, pp. 22 179–22 188, 2023.
- [26] A. Shamsi, H. Asgharnezhad, A. Tajally, S. Nahavandi, and H. Leung, “An uncertainty-aware loss function for training neural networks with calibrated predictions,” *arXiv preprint arXiv:2110.03260*, 2021.
- [27] T. Dawood, B. Ruijsink, R. Razavi, A. P. King, and E. Puyol-Antón, “Improving deep learning model calibration for cardiac applications using deterministic uncertainty networks and uncertainty-aware training,” *arXiv preprint arXiv:2405.06487*, 2024.
- [28] T. Dawood, C. Chen, B. S. Sidhu, B. Ruijsink, J. Gould, B. Porter, M. K. Elliott, V. Mehta, C. A. Rinaldi, E. Puyol-Antón *et al.*, “Uncertainty aware training to improve deep learning model calibration for classification of cardiac mr images,” *Medical Image Analysis*, vol. 88, p. 102861, 2023.
- [29] J. Jaskari, J. Sahlsten, T. Damoulas, J. Knoblauch, S. Särkkä, L. Kärkkäinen, K. Hietala, and K. K. Kaski, “Uncertainty-aware deep learning methods for robust diabetic retinopathy classification,” *IEEE Access*, vol. 10, pp. 76 669–76 681, 2022.
- [30] H. D. Kabir, S. K. Mondal, S. Khanam, A. Khosravi, S. Rahman, M. R. C. Qazani, R. Alizadehsani, H. Asadi, S. Mohamed, S. Nahavandi *et al.*, “Uncertainty aware neural network from similarity and sensitivity,” *Applied Soft Computing*, vol. 149, p. 111027, 2023.
- [31] Y. Tan, B. Jin, X. Yue, Y. Chen, and A. S. Vincentelli, “Exploiting uncertainties from ensemble learners to improve decision-making in healthcare ai,” *arXiv preprint arXiv:2007.06063*, 2020.
- [32] U. Park, Y. Kang, H. Lee, and S. Yun, “A stacking heterogeneous ensemble learning method for the prediction of building construction project costs,” *Applied sciences*, vol. 12, no. 19, p. 9729, 2022.
- [33] A. Chatzimpampas, R. M. Martins, K. Kucher, and A. Kerren, “Empirical study: visual analytics for comparing stacking to blending ensemble learning,” in *2021 23rd International Conference on Control Systems and Computer Science (CSCS)*. IEEE, 2021, pp. 1–8.
- [34] Y. Wu, H. Gunraj, C.-e. A. Tai, and A. Wong, “Covidx cxr-4: An expanded multi-institutional open-source benchmark dataset for chest x-ray image-based computer-aided covid-19 diagnostics,” *arXiv preprint arXiv:2311.17677*, 2023.
- [35] “COVIDx CXR-4 — kaggle.com,” <https://www.kaggle.com/datasets/andyczao/covidx-cxr2/data>, [Accessed 27-07-2024].
- [36] M. Tan and Q. Le, “Efficientnet: Rethinking model scaling for convolutional neural networks,” in *International conference on machine learning*. PMLR, 2019, pp. 6105–6114.
- [37] A. Kolesnikov, L. Beyer, X. Zhai, J. Puigcerver, J. Yung, S. Gelly, and N. Houlsby, “Big transfer (bit): General visual representation learning,” in *Computer Vision—ECCV 2020: 16th European Conference, Glasgow, UK, August 23–28, 2020, Proceedings, Part V 16*. Springer, 2020, pp. 491–507.
- [38] A. Dosovitskiy, L. Beyer, A. Kolesnikov, D. Weissenborn, X. Zhai, T. Unterthiner, M. Dehghani, M. Minderer, G. Heigold, S. Gelly, J. Uszkoreit, and N. Houlsby, “An image is worth 16x16 words: Transformers for image recognition at scale,” in *International Conference on Learning Representations*, 2021.

Trust-informed Decision-Making Through An Uncertainty-Aware Stacked Neural Networks Framework Case Study in COVID-19 Classification

Hassan Gharoun¹, Mohammad Sadegh Khorshidi¹, Fang Chen¹, and Amir H. Gandomi^{1,2,3}

TABLE S.I

BASE MODELS' OPTIMAL ARCHITECTURE IN MCD SETTING ACROSS VARIOUS PRE-TRAINED MODELS. EACH VALUE SPECIFIES THE NUMBER OF NEURONS IN A PARTICULAR LAYER. WHEN A SEQUENCE OF VALUES IS PROVIDED, SUCH AS (i_1, i_2, i_3) , IT INDICATES THE CONFIGURATION OF MULTIPLE HIDDEN LAYERS WITHIN THE NEURAL NETWORK ARCHITECTURE.

	BiT	E.NetB0	ViT
MCD Setting	(496, 400, 16)	(336, 336, 400, 336)	(368, 80, 432, 48, 336)

TABLE S.II

BASE MODELS' ARCHITECTURE IN ENSEMBLE AND EMCD SETTING ACROSS VARIOUS PRE-TRAINED MODELS.

	BiT	E.NetB0	ViT
Model 1	(503, 179, 176)	(218, 196, 371, 74)	(159, 436, 37)
Model 2	(299, 141)	(181, 45)	(143, 289, 323)
Model 3	(418, 123, 210, 32)	(352, 48)	(82, 44)
Model 4	(256, 380, 474)	(27, 410, 151, 489)	(194, 184, 18)
Model 5	(16, 203)	(449, 254, 413, 316)	(43, 46)
Model 6	(64, 240, 139)	(222, 177, 61)	(295, 288, 475)
Model 7	(80, 289, 173, 490)	(423, 122, 428)	(163, 314)
Model 8	(203, 294)	(508, 509)	(259, 20, 287, 492)
Model 9	(339, 134, 325, 42)	(405, 456, 408)	(339, 379, 206)
Model 10	(328, 300, 479, 72)	(32, 313, 137)	(106, 234, 453)
Model 11	(192, 467)	(314, 497)	(432, 395)
Model 12	(358, 31)	(450, 129, 18, 41)	(339, 424, 29, 165)
Model 13	(287, 483, 352)	(88, 303)	(142, 470, 359)
Model 14	(45, 378, 426, 72)	(44, 346, 289)	(163, 435)
Model 15	(231, 434, 477, 197)	(76, 213, 223)	(280, 279, 398)
Model 16	(65, 253)	(48, 374)	(151, 206)
Model 17	(261, 422, 348, 143)	(91, 276, 45)	(158, 509, 309, 243)
Model 18	(89, 337, 497, 41)	(292, 408)	(103, 369)
Model 19	(79, 174, 82, 443)	(478, 165)	(484, 110)
Model 20	(380, 158, 423, 262)	(136, 282, 511, 75)	(349, 458)
Model 21	(154, 356, 509, 206)	(97, 297, 486)	(504, 249)
Model 22	(142, 366, 373, 476)	(173, 471, 400)	(443, 236)
Model 23	(90, 160)	(373, 335, 420)	(173, 61, 73)
Model 24	(226, 27)	(209, 395, 382)	(365, 432)
Model 25	(442, 358, 353)	(506, 165)	(85, 327)
Model 26	(26, 219)	(76, 160, 182, 452)	(313, 485, 238, 27)
Model 27	(508, 503, 87)	(287, 79, 162)	(333, 271, 422)
Model 28	(362, 384)	(254, 500, 39, 103)	(209, 204)
Model 29	(222, 175, 203)	(309, 41, 386, 167)	(157, 385, 19)
Model 30	(285, 466, 96)	(61, 256, 58, 338)	(149, 437, 286)

TABLE S.III

META-MODELS OPTIMAL ARCHITECTURE ACROSS VARIOUS UQ SETTING AND PRE-TRAINED MODELS AT DIFFERENT CONFIDENCE THRESHOLDS. HERE, CONF. TH REFERS TO CONFIDENCE THRESHOLD, INC./EXC. PE STANDS FOR INCLUDING/ EXCLUDING PE AS INPUT, AND E.NETB0 REPRESENTS THE EFFICIENTNET-B0 MODEL.

Model	Input	Conf. Th	MCD Setting	Ensemble Setting	EMCD Setting
BiT	Inc. PE	0.05	(16, 240, 272, 112)	(16, 336)	(16, 368, 176, 496, 240)
E.NetB0	Inc. PE	0.05	(16, 368)	(16, 272, 464, 336)	(16, 16, 496, 240)
ViT	Inc. PE	0.05	(16, 208)	(16, 496)	(16, 400, 80)
BiT	Inc. PE	0.1	(16, 400, 48, 48, 48)	(16, 144, 112, 336)	(16, 432)
E.NetB0	Inc. PE	0.1	(16, 48, 16, 208, 48)	(16, 16, 304, 496)	(16, 304, 368, 432, 496)
ViT	Inc. PE	0.1	(16, 464)	(16, 240, 16, 16, 16)	(16, 464, 304)
BiT	Inc. PE	0.2	(176, 240)	(16, 80, 80, 80)	(16, 48, 48, 368, 304)
E.NetB0	Inc. PE	0.2	(16, 48, 400, 16)	(16, 16, 272)	(16, 80)
ViT	Inc. PE	0.2	(16, 272, 464)	(48, 432, 176)	(16, 272)
BiT	Inc. PE	0.3	(16, 272)	(144, 496, 368, 48, 80)	(16, 48, 80)
E.NetB0	Inc. PE	0.3	(16, 272)	(16, 80, 464, 176)	(464, 16, 496, 400, 16)
ViT	Inc. PE	0.3	(16, 16, 240, 144, 16)	(16, 144, 144)	(144, 432, 240, 400, 464)
BiT	Inc. PE	0.4	(16, 16, 400, 336)	(16, 112, 304, 304, 400)	(16, 496, 176)
E.NetB0	Inc. PE	0.4	(16, 240, 16, 272, 336)	(16, 304, 240, 432)	(48, 272, 304, 80)
ViT	Inc. PE	0.4	(16, 16, 304, 496)	(16, 304, 144, 16)	(496, 432, 336)
BiT	Exc. PE	0.05	(432, 336, 112, 496)	(336, 272, 176, 144, 464)	(432, 368)
E.NetB0	Exc. PE	0.05	(400, 496, 112, 400)	(272, 208, 144)	(240, 368, 368, 112, 272)
ViT	Exc. PE	0.05	(368, 400, 176)	(464, 272, 464, 208, 464)	(432, 400, 208)
BiT	Exc. PE	0.1	(432, 432, 272, 400, 464)	(400, 176, 208, 432, 496)	(368, 464, 240)
E.NetB0	Exc. PE	0.1	(464, 400, 240)	(464, 432, 80)	(432, 304, 16, 464)
ViT	Exc. PE	0.1	(432, 144, 48, 208)	(464, 144, 368, 80)	(400, 496, 368)
BiT	Exc. PE	0.2	(240, 176, 336, 400)	(336, 464, 496, 112)	(400, 368, 208, 272)
E.NetB0	Exc. PE	0.2	(400, 176, 16)	(432, 240, 400)	(432, 432, 16, 16)
ViT	Exc. PE	0.2	(336, 496, 48, 16)	(336, 432, 48, 272)	(496, 208, 400, 464, 496)
BiT	Exc. PE	0.3	(432, 80, 112, 144, 496)	(496, 432, 240)	(464, 464, 80, 80)
E.NetB0	Exc. PE	0.3	(496, 80, 48, 304, 272)	(336, 496, 48, 176)	(240, 464, 272, 336, 144)
ViT	Exc. PE	0.3	(304, 208)	(400, 432, 368, 464, 80)	(432, 464, 208)
BiT	Exc. PE	0.4	(176, 432, 336, 304)	(496, 48, 208, 304)	(336, 432, 336, 240)
E.NetB0	Exc. PE	0.4	(464, 240, 80, 208, 80)	(368, 496, 400, 112, 176)	(432, 400, 464)
ViT	Exc. PE	0.4	(464, 368, 304)	(368, 336, 368, 80, 112)	(432, 176, 496, 16)

¹Faculty of Engineering & IT, University of Technology Sydney, e-mails: Hassan.Gharoun@student.uts.edu.au, MS.khorshidialikordi@student.uts.edu.au, Fang.Chen@uts.edu.au, Gandomi@uts.edu.au.

²University Research and Innovation Center (EKIK), Óbuda University.

³Corresponding author

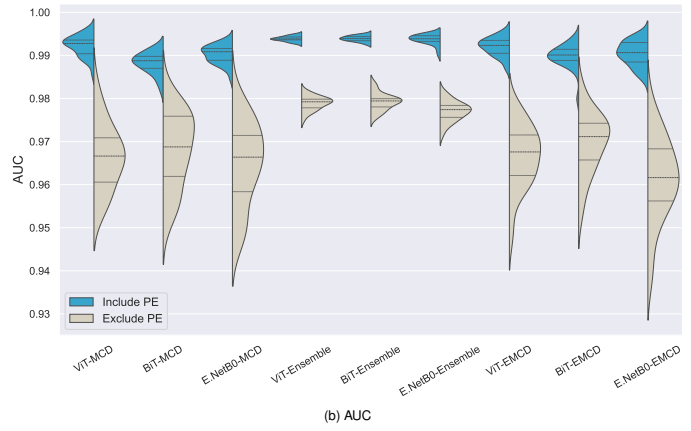
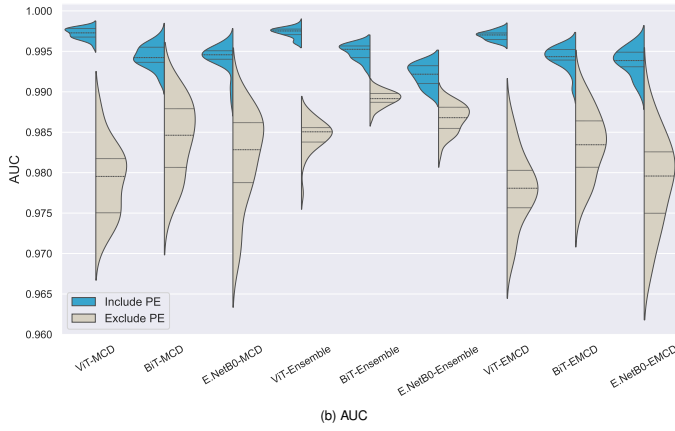
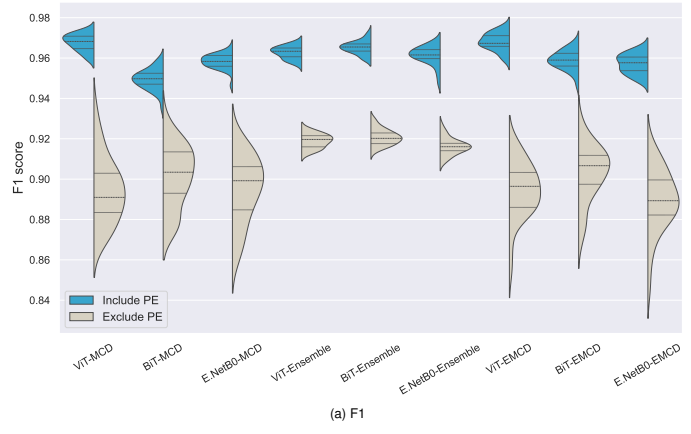
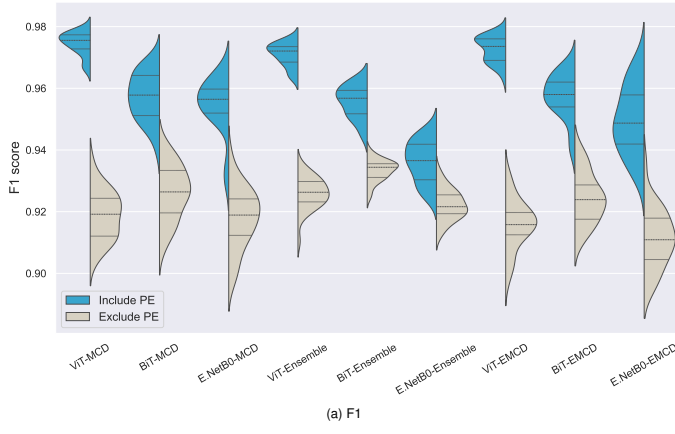


Fig. S.1. Comparative Performance of Meta-Models With and Without PE as Input at Confidence Threshold 0.05.

Fig. S.2. Comparative Performance of Meta-Models With and Without PE as Input at Confidence Threshold 0.2.

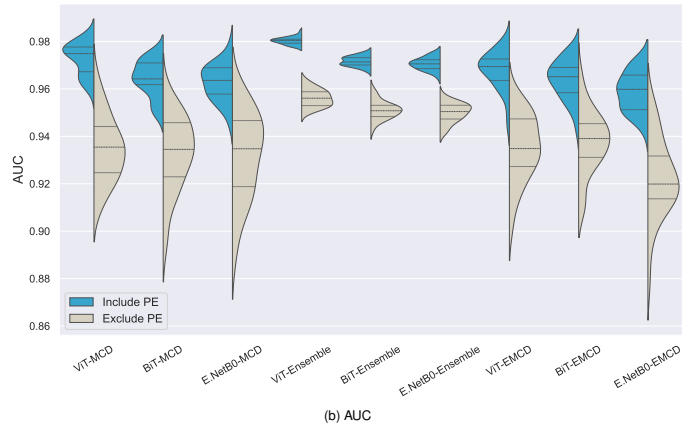
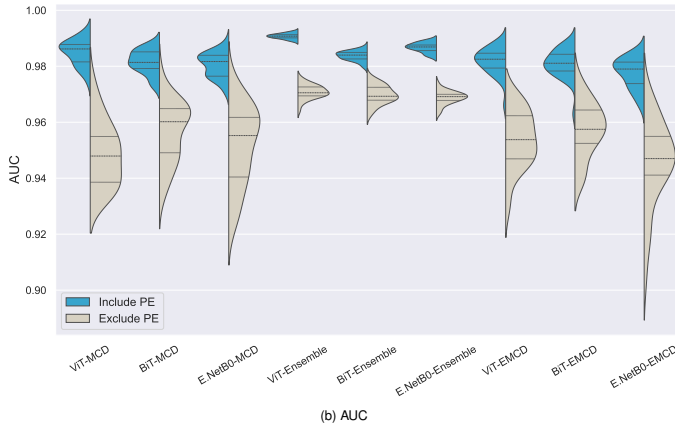
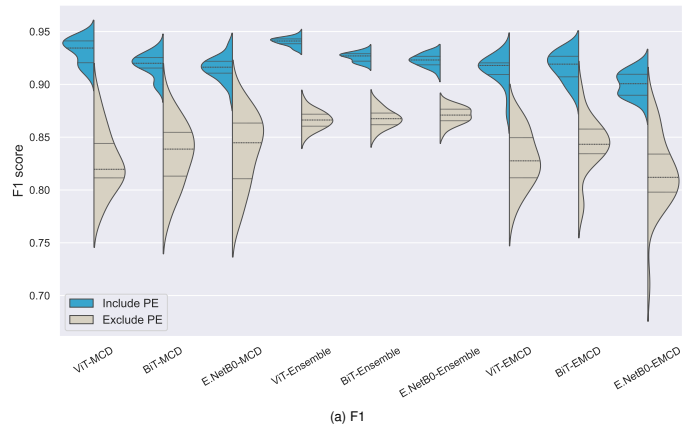
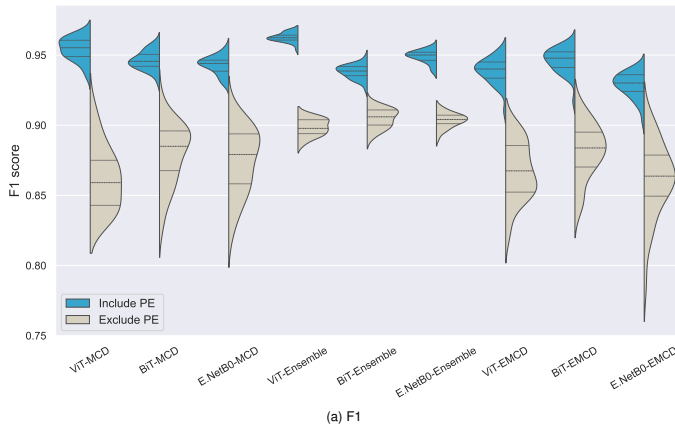


Fig. S.3. Comparative Performance of Meta-Models With and Without PE as Input at Confidence Threshold 0.3.

Fig. S.4. Comparative Performance of Meta-Models With and Without PE as Input at Confidence Threshold 0.4.

TABLE S.IV: Performance of Meta-Models Across Various Pre-trained Models across Various Confidence Thresholds of 0.05, 0.1, 0.2, 0.3, 0.4. Here, Conf. Th. refers to the confidence threshold.

Model	Approach	Conf. Th.	Include PE as input		Exclude PE as in input	
			F1 score	AUC	F1 score	AUC
BiT	MCD	0.05	%95.7212 ± 0.7485	%99.4347 ± 0.1370	%92.6210 ± 0.8632	%98.4251 ± 0.4607
BiT	Ensemble	0.05	%95.5561 ± 0.5150	%99.4923 ± 0.0949	%93.3341 ± 0.3392	%98.9156 ± 0.0921
BiT	EMCD	0.05	%95.7357 ± 0.7162	%99.4178 ± 0.1408	%92.4434 ± 0.7967	%98.3516 ± 0.4055
E.NetB0	MCD	0.05	%95.4662 ± 0.8810	%99.4180 ± 0.1597	%91.7941 ± 0.9549	%98.1787 ± 0.5566
E.NetB0	Ensemble	0.05	%93.6219 ± 0.6553	%99.2035 ± 0.1330	%92.2207 ± 0.4846	%98.6720 ± 0.1688
E.NetB0	EMCD	0.05	%94.9612 ± 1.0772	%99.3687 ± 0.1705	%91.1208 ± 0.9313	%97.8990 ± 0.5596
ViT	MCD	0.05	%97.4451 ± 0.3661	%99.7203 ± 0.0633	%91.8700 ± 0.7672	%97.8980 ± 0.4301
ViT	Ensemble	0.05	%97.0909 ± 0.3670	%99.7324 ± 0.0604	%92.5914 ± 0.5048	%98.4624 ± 0.1946
ViT	EMCD	0.05	%97.2635 ± 0.4121	%99.6925 ± 0.0543	%91.5899 ± 0.7824	%97.8060 ± 0.4355
BiT	MCD	0.1	%96.6539 ± 0.3515	%99.5043 ± 0.0949	%91.9709 ± 1.0608	%97.9825 ± 0.5543
BiT	Ensemble	0.1	%96.5189 ± 0.3838	%99.5790 ± 0.0712	%92.8740 ± 0.3631	%98.5293 ± 0.1335
BiT	EMCD	0.1	%96.4965 ± 0.4470	%99.4579 ± 0.1353	%91.7319 ± 0.9978	%97.8230 ± 0.5589
E.NetB0	MCD	0.1	%96.3704 ± 0.4546	%99.4674 ± 0.1265	%91.1689 ± 1.1750	%97.6144 ± 0.7021
E.NetB0	Ensemble	0.1	%95.7363 ± 0.5624	%99.4962 ± 0.1177	%92.2438 ± 0.4211	%98.4108 ± 0.1596
E.NetB0	EMCD	0.1	%96.0171 ± 0.5652	%99.4466 ± 0.1381	%90.6849 ± 1.1943	%97.4026 ± 0.7684
ViT	MCD	0.1	%97.4823 ± 0.3232	%99.6293 ± 0.1102	%91.0680 ± 1.1215	%97.4382 ± 0.5998
ViT	Ensemble	0.1	%97.6332 ± 0.2767	%99.7606 ± 0.0379	%92.5409 ± 0.4308	%98.2399 ± 0.1796
ViT	EMCD	0.1	%97.4426 ± 0.3090	%99.6196 ± 0.0865	%90.9633 ± 1.0366	%97.3828 ± 0.5639
BiT	MCD	0.2	%94.9300 ± 0.5068	%98.8220 ± 0.2457	%90.1056 ± 1.4910	%96.7931 ± 0.8523
BiT	Ensemble	0.2	%96.5134 ± 0.3195	%99.3890 ± 0.0633	%92.0750 ± 0.3804	%97.9211 ± 0.1942
BiT	EMCD	0.2	%95.8966 ± 0.4729	%98.9833 ± 0.2630	%90.2958 ± 1.3468	%96.9686 ± 0.6942
E.NetB0	MCD	0.2	%95.8275 ± 0.3586	%99.0163 ± 0.2119	%89.4919 ± 1.6090	%96.4757 ± 0.9531
E.NetB0	Ensemble	0.2	%96.1320 ± 0.4546	%99.3686 ± 0.1211	%91.6255 ± 0.4102	%97.7043 ± 0.2299
E.NetB0	EMCD	0.2	%95.7051 ± 0.4792	%99.0367 ± 0.2823	%88.9464 ± 1.5113	%96.1229 ± 0.9490
ViT	MCD	0.2	%96.7676 ± 0.4080	%99.2192 ± 0.2365	%89.4185 ± 1.5886	%96.6430 ± 0.7629
ViT	Ensemble	0.2	%96.2712 ± 0.3029	%99.3833 ± 0.0584	%91.8852 ± 0.3401	%97.8888 ± 0.1595
ViT	EMCD	0.2	%96.8050 ± 0.4326	%99.1961 ± 0.2123	%89.4625 ± 1.3619	%96.6492 ± 0.7179
BiT	MCD	0.3	%94.6129 ± 0.6483	%98.1506 ± 0.4176	%87.9101 ± 2.1142	%95.6322 ± 1.0661
BiT	Ensemble	0.3	%93.8041 ± 0.4859	%98.3661 ± 0.1705	%90.4776 ± 0.6763	%96.9828 ± 0.3229
BiT	EMCD	0.3	%94.5893 ± 0.8744	%98.0864 ± 0.5070	%88.1721 ± 1.8973	%95.7467 ± 0.9677
E.NetB0	MCD	0.3	%94.2817 ± 0.6380	%98.0339 ± 0.4343	%87.4330 ± 2.2644	%95.1619 ± 1.3706
E.NetB0	Ensemble	0.3	%94.8964 ± 0.4457	%98.6679 ± 0.1643	%90.3486 ± 0.5050	%96.8787 ± 0.2314
E.NetB0	EMCD	0.3	%92.8554 ± 0.8831	%97.7540 ± 0.5318	%86.1432 ± 2.5999	%94.5779 ± 1.4770
ViT	MCD	0.3	%95.4184 ± 0.8069	%98.4835 ± 0.4489	%86.1987 ± 2.2364	%94.8531 ± 1.1361
ViT	Ensemble	0.3	%96.2585 ± 0.3221	%99.0719 ± 0.0908	%89.8521 ± 0.5889	%97.0849 ± 0.2443
ViT	EMCD	0.3	%93.8658 ± 0.9028	%98.1750 ± 0.4725	%86.7271 ± 1.9921	%95.3876 ± 1.0041
BiT	MCD	0.4	%91.8368 ± 1.0582	%96.4293 ± 0.7452	%83.3265 ± 2.9670	%93.2880 ± 1.5239
BiT	Ensemble	0.4	%92.5822 ± 0.4230	%97.1638 ± 0.2006	%86.7688 ± 0.8524	%95.1074 ± 0.3707
BiT	EMCD	0.4	%91.6986 ± 1.3392	%96.3953 ± 0.8139	%84.3102 ± 2.5355	%93.7683 ± 1.2897
E.NetB0	MCD	0.4	%91.5200 ± 1.0832	%96.2633 ± 0.7640	%83.7980 ± 3.3266	%93.1960 ± 1.7735
E.NetB0	Ensemble	0.4	%92.2745 ± 0.5744	%97.0572 ± 0.2562	%87.0589 ± 0.7651	%95.0022 ± 0.3929
E.NetB0	EMCD	0.4	%90.0234 ± 1.1684	%95.8724 ± 0.8218	%81.6908 ± 3.4199	%92.2658 ± 1.6226
ViT	MCD	0.4	%93.1786 ± 1.1760	%97.2789 ± 0.6639	%82.6329 ± 2.8797	%93.4718 ± 1.3513
ViT	Ensemble	0.4	%94.0451 ± 0.3876	%98.0250 ± 0.1489	%86.6311 ± 0.8432	%95.6129 ± 0.3556
ViT	EMCD	0.4	%91.3530 ± 1.4460	%96.7970 ± 0.7829	%82.9140 ± 2.5740	%93.5298 ± 1.3446

TABLE S.V: DETAIL OF TRUST-INFORMED CRITERIA ACROSS VARIOUS PRE-TRAINED MODELS ACROSS VARIOUS CONFIDENCE THRESHOLDS OF 0.05, 0.1, 0.2, 0.3, 0.4. HERE, C. TH. REFERS TO CONFIDENCE THRESHOLD, INC./EXC. PE STANDS FOR INCLUDING/ EXCLUDING PE AS INPUT, AND E.NETB0 REPRESENTS THE EFFICIENTNET-B0 MODEL.

Pretrained	UQ Setting	Input	C. Th	CAR	CPR	TPR	FTR	RAR	MRR	TTR	FRR
BIT	MCD	Inc. PE	0.05	% 27.61 ± 4.59	% 30.34 ± 5.01	% 93.60 ± 1.55	% 0.21 ± 0.08	% 70.55 ± 4.56	% 85.15 ± 0.81	% 12.52 ± 0.65	% 2.33 ± 0.45
BIT	MCD	Inc. PE	0.1	% 37.06 ± 5.00	% 40.73 ± 5.44	% 95.49 ± 0.77	% 0.44 ± 0.15	% 61.20 ± 5.09	% 83.62 ± 1.06	% 14.08 ± 0.84	% 2.30 ± 0.46
BIT	MCD	Inc. PE	0.2	% 50.07 ± 5.01	% 55.02 ± 5.43	% 94.57 ± 0.65	% 1.12 ± 0.30	% 47.05 ± 5.36	% 78.58 ± 1.55	% 16.90 ± 1.15	% 4.51 ± 0.90
BIT	MCD	Inc. PE	0.3	% 61.70 ± 4.21	% 67.81 ± 4.55	% 94.86 ± 0.48	% 2.08 ± 0.39	% 34.96 ± 4.41	% 75.49 ± 1.84	% 20.00 ± 1.27	% 4.50 ± 0.83
BIT	MCD	Inc. PE	0.4	% 71.16 ± 3.26	% 78.21 ± 3.50	% 94.03 ± 0.44	% 3.31 ± 0.46	% 24.31 ± 3.57	% 69.59 ± 2.11	% 23.69 ± 1.51	% 6.72 ± 1.12
BIT	MCD	Exc. PE	0.05	% 26.40 ± 4.68	% 29.02 ± 5.12	% 89.35 ± 1.69	% 0.31 ± 0.18	% 70.42 ± 5.40	% 83.33 ± 1.76	% 12.44 ± 0.66	% 4.23 ± 1.27
BIT	MCD	Exc. PE	0.1	% 35.36 ± 5.11	% 38.87 ± 5.57	% 89.42 ± 1.19	% 0.65 ± 0.29	% 60.41 ± 5.99	% 80.35 ± 3.02	% 13.96 ± 0.83	% 5.69 ± 1.49
BIT	MCD	Exc. PE	0.2	% 48.64 ± 4.78	% 53.46 ± 5.20	% 89.84 ± 1.39	% 1.49 ± 0.44	% 45.72 ± 5.54	% 74.28 ± 2.16	% 16.61 ± 0.97	% 9.11 ± 2.29
BIT	MCD	Exc. PE	0.3	% 59.86 ± 4.52	% 65.80 ± 4.90	% 89.93 ± 1.47	% 2.61 ± 0.66	% 33.38 ± 5.66	% 68.47 ± 3.23	% 19.43 ± 1.23	% 12.10 ± 2.51
BIT	MCD	Exc. PE	0.4	% 69.64 ± 3.30	% 76.55 ± 3.57	% 89.24 ± 1.51	% 4.13 ± 0.66	% 21.93 ± 4.15	% 60.72 ± 4.58	% 22.55 ± 1.58	% 16.73 ± 4.23
BIT	Ensemble	Inc. PE	0.05	% 21.42 ± 0.88	% 23.40 ± 0.95	% 92.92 ± 1.23	% 0.06 ± 0.02	% 76.95 ± 0.87	% 87.10 ± 0.41	% 10.93 ± 0.27	% 1.96 ± 0.29
BIT	Ensemble	Inc. PE	0.1	% 30.66 ± 1.07	% 33.50 ± 1.15	% 95.04 ± 0.84	% 0.18 ± 0.03	% 67.74 ± 1.01	% 85.63 ± 0.48	% 12.25 ± 0.31	% 2.12 ± 0.35
BIT	Ensemble	Inc. PE	0.2	% 45.71 ± 1.09	% 49.95 ± 1.19	% 95.81 ± 0.65	% 0.62 ± 0.06	% 52.29 ± 1.15	% 82.15 ± 0.77	% 15.03 ± 0.43	% 2.82 ± 0.56
BIT	Ensemble	Inc. PE	0.3	% 58.01 ± 1.19	% 63.38 ± 1.30	% 94.27 ± 0.64	% 1.48 ± 0.14	% 38.46 ± 1.41	% 75.67 ± 0.90	% 18.20 ± 0.64	% 6.13 ± 0.88
BIT	Ensemble	Inc. PE	0.4	% 70.34 ± 0.93	% 76.85 ± 1.04	% 94.40 ± 0.50	% 2.73 ± 0.18	% 25.49 ± 1.22	% 71.07 ± 1.33	% 22.56 ± 0.91	% 6.38 ± 1.23
BIT	Ensemble	Exc. PE	0.05	% 20.48 ± 1.03	% 22.38 ± 1.12	% 89.24 ± 1.63	% 0.09 ± 0.02	% 77.04 ± 1.37	% 86.21 ± 0.43	% 10.93 ± 0.20	% 2.87 ± 0.45
BIT	Ensemble	Exc. PE	0.1	% 28.74 ± 1.22	% 31.41 ± 1.31	% 90.05 ± 1.56	% 0.23 ± 0.05	% 68.07 ± 1.64	% 83.46 ± 0.66	% 12.15 ± 0.26	% 4.39 ± 0.64
BIT	Ensemble	Exc. PE	0.2	% 43.36 ± 1.38	% 47.39 ± 1.49	% 90.69 ± 1.25	% 0.75 ± 0.20	% 52.17 ± 1.78	% 78.58 ± 1.01	% 14.86 ± 0.41	% 6.56 ± 1.14
BIT	Ensemble	Exc. PE	0.3	% 56.52 ± 1.28	% 61.77 ± 1.41	% 91.03 ± 1.22	% 1.71 ± 0.10	% 37.89 ± 1.92	% 72.98 ± 1.26	% 17.94 ± 0.56	% 9.09 ± 1.40
BIT	Ensemble	Exc. PE	0.4	% 68.85 ± 0.96	% 75.25 ± 1.07	% 90.30 ± 0.80	% 3.31 ± 0.27	% 23.75 ± 1.41	% 66.45 ± 1.51	% 21.89 ± 0.75	% 11.66 ± 1.59
BIT	EMCD	Inc. PE	0.05	% 28.56 ± 4.36	% 31.39 ± 4.79	% 93.68 ± 1.42	% 0.23 ± 0.10	% 69.54 ± 4.41	% 84.95 ± 0.78	% 12.68 ± 0.76	% 2.36 ± 0.43
BIT	EMCD	Inc. PE	0.1	% 37.86 ± 4.58	% 41.62 ± 5.04	% 95.37 ± 0.87	% 0.49 ± 0.19	% 60.30 ± 4.79	% 83.33 ± 1.08	% 14.21 ± 0.96	% 2.46 ± 0.44
BIT	EMCD	Inc. PE	0.2	% 51.36 ± 4.21	% 56.45 ± 4.63	% 95.32 ± 0.65	% 1.19 ± 0.31	% 46.12 ± 4.48	% 79.59 ± 1.61	% 17.08 ± 1.16	% 3.33 ± 0.69
BIT	EMCD	Inc. PE	0.3	% 62.17 ± 3.69	% 68.34 ± 4.07	% 94.83 ± 0.55	% 2.13 ± 0.43	% 34.43 ± 4.10	% 75.48 ± 2.02	% 20.17 ± 1.38	% 4.35 ± 1.13
BIT	EMCD	Inc. PE	0.4	% 71.12 ± 2.97	% 78.18 ± 3.29	% 94.01 ± 0.56	% 3.31 ± 0.49	% 24.33 ± 3.46	% 69.23 ± 2.69	% 23.69 ± 1.63	% 7.08 ± 1.56
BIT	EMCD	Exc. PE	0.05	% 26.35 ± 3.50	% 28.98 ± 3.84	% 89.22 ± 1.68	% 0.29 ± 0.12	% 70.43 ± 4.15	% 83.09 ± 1.48	% 12.53 ± 0.58	% 4.37 ± 1.06
BIT	EMCD	Exc. PE	0.1	% 34.65 ± 3.88	% 38.11 ± 4.26	% 89.49 ± 1.26	% 0.60 ± 0.21	% 61.26 ± 4.52	% 79.96 ± 2.05	% 13.92 ± 0.75	% 6.13 ± 1.59
BIT	EMCD	Exc. PE	0.2	% 48.03 ± 4.68	% 52.84 ± 5.14	% 89.22 ± 1.35	% 1.46 ± 0.42	% 46.12 ± 5.68	% 75.19 ± 2.32	% 16.69 ± 1.21	% 8.12 ± 1.70
BIT	EMCD	Exc. PE	0.3	% 58.82 ± 4.44	% 64.71 ± 4.87	% 89.64 ± 1.39	% 2.49 ± 0.59	% 34.34 ± 5.38	% 69.20 ± 3.04	% 19.43 ± 1.44	% 11.38 ± 2.33
BIT	EMCD	Exc. PE	0.4	% 68.39 ± 3.73	% 75.23 ± 4.08	% 89.48 ± 1.09	% 3.85 ± 0.67	% 23.55 ± 3.77	% 61.52 ± 4.04	% 22.53 ± 1.61	% 15.95 ± 3.23
E.NetB0	MCD	Inc. PE	0.05	% 25.52 ± 3.80	% 28.29 ± 4.18	% 92.93 ± 1.59	% 0.22 ± 0.09	% 72.59 ± 3.97	% 84.50 ± 0.67	% 13.26 ± 0.53	% 2.24 ± 0.45
E.NetB0	MCD	Inc. PE	0.1	% 34.32 ± 3.84	% 38.06 ± 4.21	% 94.92 ± 0.92	% 0.48 ± 0.15	% 63.85 ± 3.97	% 82.98 ± 0.86	% 14.68 ± 0.64	% 2.34 ± 0.47
E.NetB0	MCD	Inc. PE	0.2	% 47.56 ± 4.03	% 52.73 ± 4.41	% 94.96 ± 0.50	% 1.20 ± 0.26	% 49.92 ± 4.22	% 79.39 ± 1.23	% 17.33 ± 0.83	% 3.27 ± 0.71
E.NetB0	MCD	Inc. PE	0.3	% 58.42 ± 4.01	% 64.79 ± 4.36	% 94.48 ± 0.49	% 2.19 ± 0.38	% 38.15 ± 4.36	% 74.71 ± 1.81	% 20.12 ± 1.11	% 5.16 ± 1.06
E.NetB0	MCD	Inc. PE	0.4	% 68.18 ± 3.55	% 75.61 ± 3.85	% 93.42 ± 0.65	% 3.45 ± 0.46	% 27.01 ± 3.93	% 68.76 ± 2.58	% 23.79 ± 1.53	% 7.45 ± 1.54
E.NetB0	MCD	Exc. PE	0.05	% 23.27 ± 4.85	% 25.78 ± 5.37	% 88.02 ± 2.29	% 0.32 ± 0.19	% 73.53 ± 5.71	% 82.75 ± 1.95	% 12.90 ± 0.75	% 4.35 ± 1.33
E.NetB0	MCD	Exc. PE	0.1	% 31.12 ± 5.41	% 34.49 ± 5.98	% 87.90 ± 1.83	% 0.66 ± 0.34	% 64.55 ± 6.38	% 80.05 ± 2.31	% 14.18 ± 0.88	% 5.77 ± 1.62
E.NetB0	MCD	Exc. PE	0.2	% 43.60 ± 5.60	% 48.32 ± 6.20	% 88.11 ± 1.81	% 1.51 ± 0.57	% 50.46 ± 6.70	% 74.56 ± 2.89	% 16.48 ± 1.14	% 8.96 ± 2.06
E.NetB0	MCD	Exc. PE	0.3	% 55.05 ± 5.12	% 61.00 ± 5.67	% 88.35 ± 1.67	% 2.60 ± 0.74	% 37.65 ± 6.10	% 68.69 ± 3.79	% 19.20 ± 1.42	% 12.11 ± 3.17
E.NetB0	MCD	Exc. PE	0.4	% 65.74 ± 4.38	% 72.86 ± 4.86	% 88.40 ± 1.93	% 4.07 ± 0.92	% 25.56 ± 5.59	% 61.38 ± 3.79	% 22.56 ± 1.82	% 16.06 ± 2.92
E.NetB0	Ensemble	Inc. PE	0.05	% 16.13 ± 0.92	% 17.77 ± 1.00	% 90.15 ± 1.59	% 0.04 ± 0.01	% 82.10 ± 0.95	% 86.43 ± 0.40	% 11.14 ± 0.19	% 2.43 ± 0.40
E.NetB0	Ensemble	Inc. PE	0.1	% 25.07 ± 1.02	% 27.61 ± 1.10	% 93.83 ± 1.08	% 0.13 ± 0.02	% 73.28 ± 0.95	% 85.34 ± 0.45	% 12.36 ± 0.21	% 2.30 ± 0.38
E.NetB0	Ensemble	Inc. PE	0.2	% 40.83 ± 1.07	% 44.96 ± 1.15	% 95.06 ± 0.88	% 0.58 ± 0.07	% 57.05 ± 1.06	% 81.99 ± 0.57	% 15.10 ± 0.30	% 2.91 ± 0.47
E.NetB0	Ensemble	Inc. PE	0.3	% 55.04 ± 0.94	% 60.61 ± 1.00	% 94.86 ± 0.61	% 1.45 ± 0.11	% 41.97 ± 1.02	% 76.80 ± 0.77	% 18.44 ± 0.39	% 4.76 ± 0.67
E.NetB0	Ensemble	Inc. PE	0.4	% 67.54 ± 0.79	% 74.37 ± 0.81	% 93.93 ± 0.53	% 2.81 ± 0.15	% 28.09 ± 1.00	% 70.10 ± 1.44	% 22.70 ± 0.46	% 7.20 ± 1.42
E.NetB0	Ensemble	Exc. PE	0.05	% 16.00 ± 0.86	% 17.61 ± 0.94	% 88.45 ± 1.82	% 0.05 ± 0.02	% 81.90 ± 1.18	% 85.76 ± 0.51	% 11.13 ± 0.28	% 3.11 ± 0.53
E.NetB0	Ensemble	Exc. PE	0.1	% 24.15 ± 1.27	% 26.59 ± 1.39	% 89.10 ± 1.79	% 0.19 ± 0.04	% 72.87 ± 1.73	% 83.35 ± 0.58	% 12.32 ± 0.37	% 4.33 ± 0.77
E.NetB0	Ensemble	Exc. PE	0.2	% 39.12 ± 1.38	% 43.07 ± 1.49	% 89.90 ± 1.39	% 0.77 ± 0.12	% 56.46 ± 1.89	% 78.41 ± 0.93	% 14.88 ± 0.39	% 6.71 ± 1.03
E.NetB0	Ensemble	Exc. PE	0.3	% 53.84 ± 1.31	% 59.27 ± 1.41	% 90.10 ± 1.11	% 1.85 ± 0.18	% 40.23 ± 1.81	% 73.30 ± 1.08	% 18.20 ± 0.57	% 8.49 ± 1.27
E.NetB0	Ensemble	Exc. PE	0.4	% 66.51 ± 1.44	% 73.22 ± 1.59	% 90.23 ± 1.02	% 3.37 ± 0.31	% 26.27 ± 2.17	% 65.63 ± 1.84	% 22.15 ± 1.08	% 12.22 ± 2.61

TABLE S.V: DETAIL OF TRUST-INFORMED CRITERIA ACROSS VARIOUS PRE-TRAINED MODELS ACROSS VARIOUS CONFIDENCE THRESHOLDS OF 0.05, 0.1, 0.2, 0.3, 0.4. HERE, C. TH. REFERS TO CONFIDENCE THRESHOLD, INC./EXC. PE STANDS FOR INCLUDING/ EXCLUDING PE AS INPUT, AND E.NETB0 REPRESENTS THE EFFICIENTNET-B0 MODEL.

Pretrained	UQ Setting	Input	C. Th	CAR	CPR	TPR	FTR	RAR	MRR	TTR	FRR
E.NetB0	EMCD	Inc. PE	0.05	% 22.33 ± 5.40	% 24.78 ± 5.94	% 92.44 ± 1.92	% 0.17 ± 0.09	% 75.92 ± 5.42	% 84.79 ± 0.80	% 12.85 ± 0.69	% 2.36 ± 0.44
E.NetB0	EMCD	Inc. PE	0.1	% 31.30 ± 5.70	% 34.73 ± 6.27	% 94.00 ± 0.86	% 0.42 ± 0.18	% 66.72 ± 5.95	% 83.50 ± 1.13	% 14.27 ± 0.90	% 2.23 ± 0.56
E.NetB0	EMCD	Inc. PE	0.2	% 45.01 ± 5.65	% 49.94 ± 6.21	% 94.69 ± 0.61	% 1.11 ± 0.34	% 52.46 ± 6.00	% 79.88 ± 1.64	% 16.85 ± 1.19	% 3.27 ± 0.64
E.NetB0	EMCD	Inc. PE	0.3	% 56.54 ± 4.88	% 62.74 ± 5.37	% 92.60 ± 0.99	% 2.16 ± 0.46	% 38.95 ± 5.17	% 74.11 ± 2.66	% 20.01 ± 1.45	% 5.88 ± 1.57
E.NetB0	EMCD	Inc. PE	0.4	% 66.79 ± 3.79	% 74.12 ± 4.19	% 92.46 ± 0.68	% 3.45 ± 0.53	% 27.75 ± 4.15	% 66.82 ± 3.03	% 23.44 ± 1.76	% 9.74 ± 1.82
E.NetB0	EMCD	Exc. PE	0.05	% 22.49 ± 4.19	% 24.95 ± 4.62	% 87.05 ± 1.74	% 0.34 ± 0.27	% 74.14 ± 4.93	% 82.39 ± 1.81	% 12.94 ± 0.60	% 4.67 ± 1.37
E.NetB0	EMCD	Exc. PE	0.1	% 30.79 ± 4.91	% 34.15 ± 5.41	% 87.66 ± 2.13	% 0.60 ± 0.17	% 64.82 ± 5.88	% 79.39 ± 2.26	% 14.31 ± 0.83	% 6.30 ± 1.66
E.NetB0	EMCD	Exc. PE	0.2	% 43.98 ± 5.33	% 48.79 ± 5.86	% 87.95 ± 1.64	% 1.53 ± 0.52	% 49.94 ± 6.42	% 73.34 ± 3.16	% 16.81 ± 1.07	% 9.85 ± 2.42
E.NetB0	EMCD	Exc. PE	0.3	% 56.14 ± 5.20	% 62.28 ± 5.71	% 87.32 ± 1.77	% 2.89 ± 0.80	% 35.63 ± 6.65	% 67.33 ± 3.89	% 19.79 ± 1.36	% 12.88 ± 3.20
E.NetB0	EMCD	Exc. PE	0.4	% 66.70 ± 4.52	% 74.00 ± 4.94	% 87.27 ± 1.66	% 4.53 ± 0.93	% 23.51 ± 5.74	% 59.49 ± 4.52	% 22.98 ± 1.75	% 17.53 ± 3.42
VIT	MCD	Inc. PE	0.05	% 38.01 ± 5.86	% 41.48 ± 6.36	% 96.61 ± 0.74	% 0.22 ± 0.10	% 60.69 ± 5.91	% 84.67 ± 1.15	% 13.54 ± 1.07	% 1.79 ± 0.51
VIT	MCD	Inc. PE	0.1	% 46.85 ± 5.48	% 51.13 ± 5.94	% 96.91 ± 0.51	% 0.46 ± 0.17	% 51.67 ± 5.61	% 82.60 ± 1.47	% 15.45 ± 1.26	% 1.94 ± 0.40
VIT	MCD	Inc. PE	0.2	% 58.14 ± 4.65	% 63.45 ± 5.02	% 96.74 ± 0.46	% 1.03 ± 0.27	% 39.90 ± 4.83	% 78.60 ± 1.90	% 18.58 ± 1.44	% 2.83 ± 0.75
VIT	MCD	Inc. PE	0.3	% 66.59 ± 3.66	% 72.67 ± 3.94	% 96.22 ± 0.46	% 1.75 ± 0.34	% 30.79 ± 3.95	% 74.10 ± 2.46	% 25.38 ± 1.82	% 4.19 ± 1.33
VIT	MCD	Inc. PE	0.4	% 73.79 ± 2.94	% 80.54 ± 3.16	% 95.50 ± 0.56	% 2.67 ± 0.45	% 22.72 ± 3.40	% 68.57 ± 2.38	% 25.38 ± 1.82	% 6.05 ± 1.25
VIT	MCD	Exc. PE	0.05	% 36.80 ± 5.32	% 40.17 ± 5.79	% 89.78 ± 1.28	% 0.41 ± 0.15	% 59.01 ± 5.92	% 80.20 ± 2.19	% 13.63 ± 1.06	% 6.17 ± 1.38
VIT	MCD	Exc. PE	0.1	% 45.52 ± 5.14	% 49.69 ± 5.57	% 90.34 ± 1.32	% 0.78 ± 0.27	% 49.57 ± 5.95	% 76.46 ± 2.58	% 15.49 ± 1.22	% 8.05 ± 1.69
VIT	MCD	Exc. PE	0.2	% 57.29 ± 4.42	% 62.54 ± 4.77	% 90.64 ± 1.34	% 1.64 ± 0.43	% 36.71 ± 5.29	% 70.90 ± 3.34	% 18.58 ± 1.33	% 10.53 ± 2.47
VIT	MCD	Exc. PE	0.3	% 65.08 ± 3.98	% 71.04 ± 4.27	% 90.64 ± 1.34	% 2.55 ± 0.55	% 28.16 ± 4.95	% 62.97 ± 3.93	% 20.99 ± 1.50	% 16.04 ± 3.19
VIT	MCD	Exc. PE	0.4	% 73.36 ± 3.21	% 80.08 ± 3.43	% 90.13 ± 1.03	% 3.79 ± 0.63	% 18.59 ± 3.96	% 57.29 ± 4.28	% 25.09 ± 1.82	% 17.61 ± 3.21
VIT	Ensemble	Inc. PE	0.05	% 30.80 ± 1.08	% 33.34 ± 1.16	% 95.87 ± 0.78	% 0.06 ± 0.02	% 67.88 ± 1.02	% 87.09 ± 0.42	% 11.14 ± 0.26	% 1.77 ± 0.36
VIT	Ensemble	Inc. PE	0.1	% 41.00 ± 1.17	% 44.38 ± 1.25	% 97.22 ± 0.49	% 0.17 ± 0.03	% 57.83 ± 1.17	% 85.16 ± 0.43	% 12.89 ± 0.31	% 1.96 ± 0.36
VIT	Ensemble	Inc. PE	0.2	% 54.27 ± 1.11	% 58.75 ± 1.18	% 96.28 ± 0.60	% 0.56 ± 0.06	% 43.63 ± 1.19	% 80.21 ± 0.64	% 16.20 ± 0.42	% 3.59 ± 0.64
VIT	Ensemble	Inc. PE	0.3	% 65.21 ± 0.84	% 70.59 ± 0.90	% 96.78 ± 0.48	% 1.20 ± 0.10	% 32.62 ± 0.89	% 76.80 ± 0.68	% 19.70 ± 0.48	% 3.50 ± 0.71
VIT	Ensemble	Inc. PE	0.4	% 73.86 ± 0.84	% 79.96 ± 0.87	% 95.94 ± 0.30	% 2.09 ± 0.13	% 23.01 ± 0.90	% 70.69 ± 1.14	% 24.06 ± 0.63	% 5.25 ± 1.34
VIT	Ensemble	Exc. PE	0.05	% 28.47 ± 1.21	% 30.82 ± 1.30	% 89.47 ± 1.69	% 0.11 ± 0.03	% 68.16 ± 1.61	% 84.53 ± 0.67	% 11.02 ± 0.30	% 4.45 ± 0.74
VIT	Ensemble	Exc. PE	0.1	% 38.33 ± 1.07	% 41.49 ± 1.14	% 90.77 ± 1.10	% 0.27 ± 0.05	% 57.77 ± 1.38	% 81.48 ± 0.88	% 12.72 ± 0.32	% 5.80 ± 0.95
VIT	Ensemble	Exc. PE	0.2	% 52.61 ± 0.97	% 56.95 ± 1.03	% 91.38 ± 0.94	% 0.80 ± 0.10	% 42.41 ± 1.41	% 76.89 ± 1.05	% 16.08 ± 0.43	% 7.03 ± 1.19
VIT	Ensemble	Exc. PE	0.3	% 63.42 ± 0.79	% 68.65 ± 0.83	% 91.27 ± 0.89	% 1.67 ± 0.17	% 30.51 ± 1.22	% 71.43 ± 1.31	% 19.50 ± 0.55	% 9.07 ± 1.48
VIT	Ensemble	Exc. PE	0.4	% 72.33 ± 0.77	% 78.30 ± 0.80	% 91.42 ± 0.87	% 2.79 ± 0.24	% 20.86 ± 1.36	% 64.29 ± 1.71	% 23.15 ± 0.75	% 12.56 ± 1.96
VIT	EMCD	Inc. PE	0.1	% 37.14 ± 4.68	% 40.51 ± 5.04	% 96.37 ± 0.80	% 0.22 ± 0.07	% 61.48 ± 4.69	% 84.87 ± 0.66	% 13.23 ± 0.78	% 1.90 ± 0.39
VIT	EMCD	Inc. PE	0.2	% 46.67 ± 4.44	% 50.90 ± 4.77	% 96.86 ± 0.59	% 0.47 ± 0.13	% 51.82 ± 4.57	% 82.80 ± 1.06	% 15.23 ± 0.91	% 1.97 ± 0.38
VIT	EMCD	Inc. PE	0.3	% 58.75 ± 4.04	% 64.07 ± 4.30	% 96.80 ± 0.35	% 1.08 ± 0.25	% 39.31 ± 4.24	% 78.68 ± 1.60	% 18.54 ± 1.18	% 2.78 ± 0.84
VIT	EMCD	Inc. PE	0.4	% 67.17 ± 3.65	% 73.26 ± 3.87	% 95.01 ± 0.60	% 1.93 ± 0.37	% 29.29 ± 3.97	% 72.61 ± 2.34	% 21.99 ± 1.51	% 5.39 ± 1.39
VIT	EMCD	Inc. PE	0.05	% 73.94 ± 2.92	% 80.65 ± 3.07	% 94.96 ± 0.65	% 2.78 ± 0.43	% 22.13 ± 3.17	% 65.15 ± 3.51	% 25.23 ± 1.54	% 9.62 ± 2.74
VIT	EMCD	Exc. PE	0.1	% 34.41 ± 4.40	% 37.54 ± 4.77	% 89.54 ± 1.43	% 0.34 ± 0.15	% 61.55 ± 5.06	% 80.58 ± 1.99	% 13.07 ± 0.80	% 6.35 ± 1.42
VIT	EMCD	Exc. PE	0.2	% 43.85 ± 4.40	% 47.84 ± 4.76	% 89.83 ± 1.29	% 0.70 ± 0.25	% 51.15 ± 5.27	% 77.17 ± 2.20	% 15.04 ± 1.03	% 7.79 ± 1.54
VIT	EMCD	Exc. PE	0.3	% 55.89 ± 3.62	% 60.98 ± 3.89	% 90.62 ± 1.16	% 1.46 ± 0.35	% 38.31 ± 4.26	% 71.00 ± 3.14	% 18.07 ± 1.07	% 10.93 ± 2.56
VIT	EMCD	Exc. PE	0.4	% 64.96 ± 3.11	% 70.87 ± 3.33	% 90.33 ± 1.20	% 2.49 ± 0.47	% 28.06 ± 3.87	% 64.80 ± 3.52	% 21.01 ± 1.26	% 14.20 ± 3.02
VIT	EMCD	Exc. PE	0.4	% 72.57 ± 2.61	% 79.17 ± 2.79	% 90.14 ± 1.09	% 3.68 ± 0.58	% 19.48 ± 3.38	% 57.81 ± 3.44	% 24.11 ± 1.32	% 18.08 ± 2.98

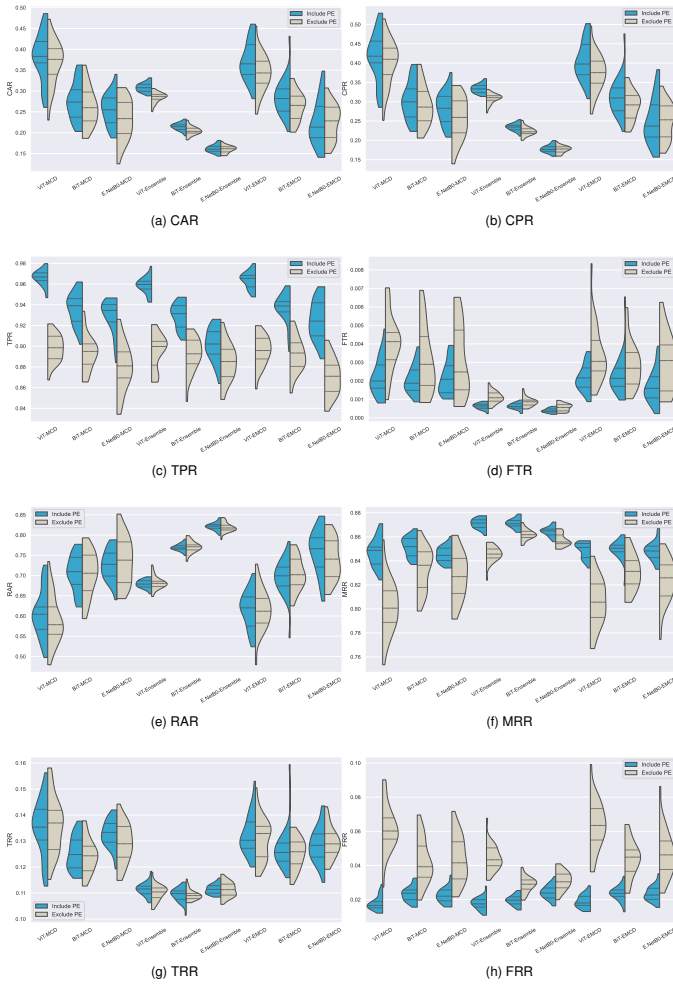


Fig. S.5. Comparison of Uncertainty-Informed Criteria Across Pre-trained Models at a Confidence Threshold of 0.05, With and Without PE as Input.

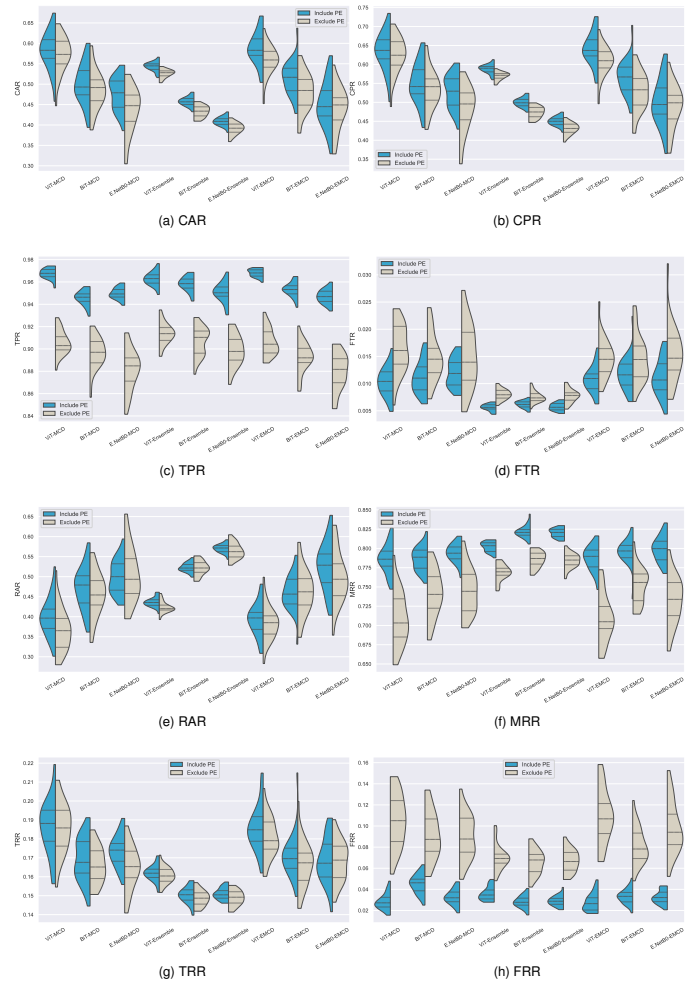


Fig. S.6. Comparison of Uncertainty-Informed Criteria Across Pre-trained Models at a Confidence Threshold of 0.2, With and Without PE as Input.

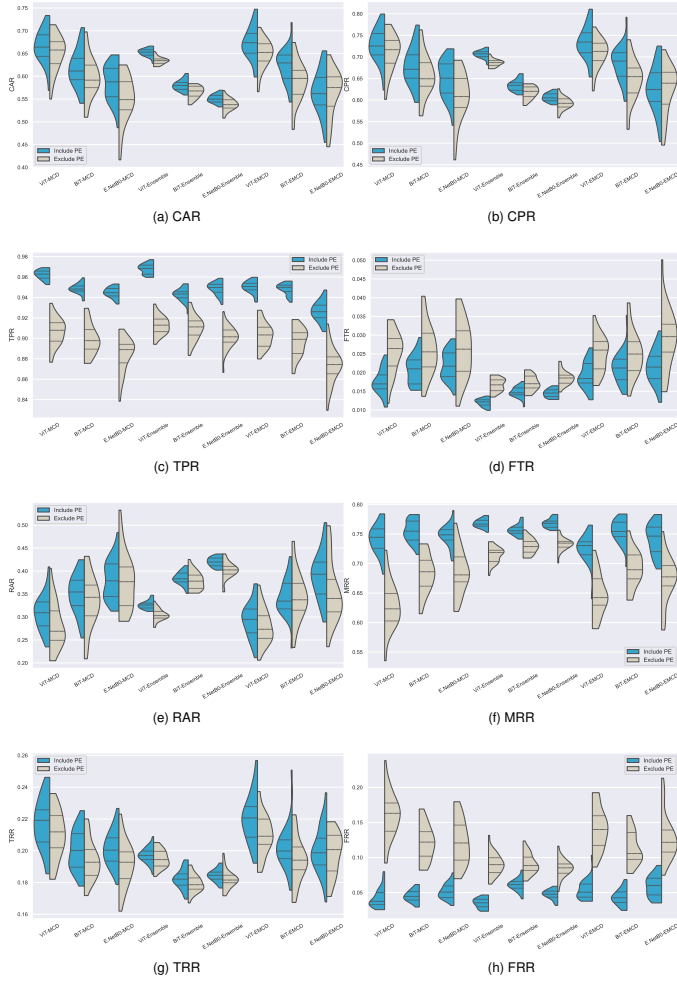


Fig. S.7. Comparison of Uncertainty-Informed Criteria Across Pre-trained Models at a Confidence Threshold of 0.3, With and Without PE as Input.

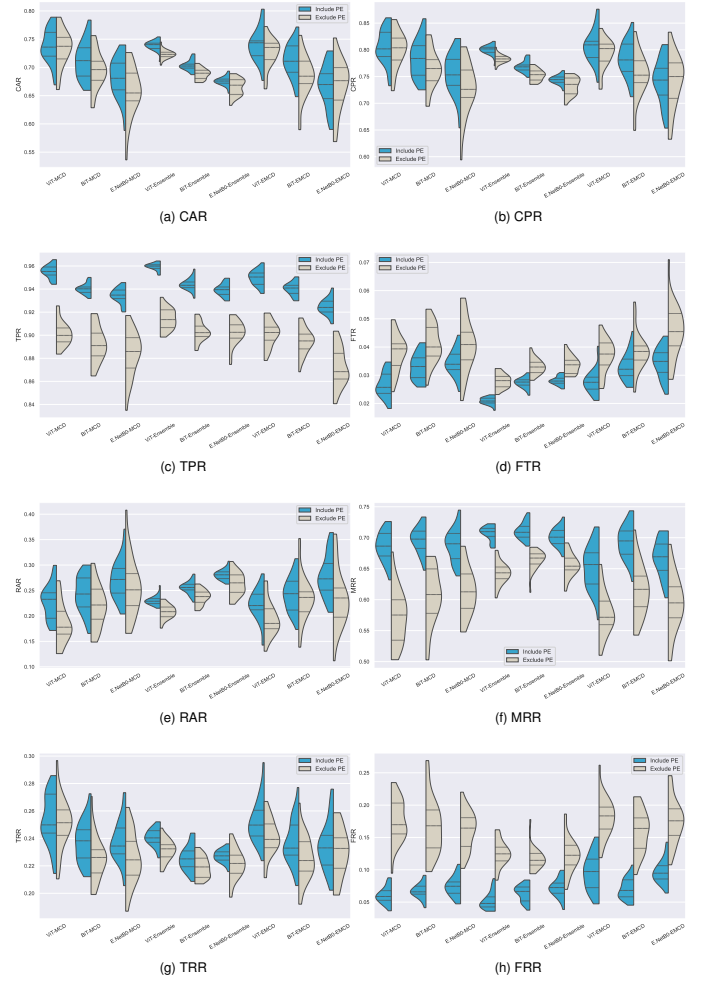


Fig. S.8. Comparison of Uncertainty-Informed Criteria Across Pre-trained Models at a Confidence Threshold of 0.4, With and Without PE as Input.